Journal of Medicinal Chemistry

pubs.acs.org/jmc

Article

Di-bromo-Based Small-Molecule Inhibitors of the PD-1/PD-L1 Immune Checkpoint

Magdalena Konieczny, Bogdan Musielak, Justyna Kocik, Lukasz Skalniak, Dominik Sala, Miroslawa Czub, Katarzyna Magiera-Mularz, Ismael Rodriguez, Maja Myrcha, Malgorzata Stec, Maciej Siedlar, Tad A. Holak,* and Jacek Plewka*

Cite This: *J. Med. Chem.* 2020, 63, 11271−11285

Read Online

ACCESS | Metrics & More | Article Recommendations | Supporting Information

ABSTRACT: Immune checkpoint blockade is one of the most promising strategies of cancer immunotherapy. However, unlike classical targeted therapies, it is currently solely based on expensive monoclonal antibodies, which often inflict immune-related adverse events. Herein, we propose a novel small-molecule inhibitor targeted at the most clinically relevant immune checkpoint, PD-1/PD-L1. The compound is capable of disrupting the PD-1/PD-L1 complex by antagonizing PD-L1 and, therefore, restores activation of T cells similarly to the antibodies, while being cheap in production and possibly nonimmunogenic. The final compound is significantly smaller than others reported in the literature while being nontoxic to cells even at high concentrations. The scaffold was designed using a structure−activity relationship screening cascade based on a new antagonist-induced dissociation NMR assay, called the weak-AIDA-NMR. Weak-AIDA-NMR finds true inhibitors, as opposed to only binders to the target protein, in early steps of lead compound development, and this process makes it less time and cost consuming.

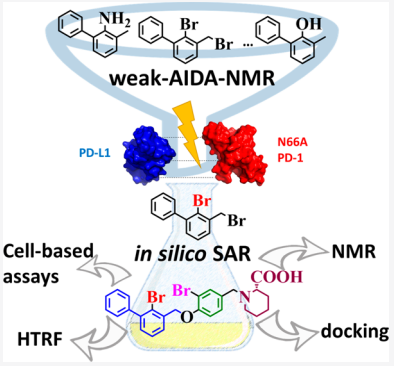

INTRODUCTION

Programmed cell death protein 1 (PD-1, known also as CD279) and its ligand (PD-L1, known also as CD274 or B7-H1) are transmembrane receptors involved in the negative regulation of the activated T cells. The interaction of PD-1 with PD-L1 induces T cell apoptosis, anergy, and functional exhaustion.[1,2] Some aggressive cancers, including breast, pancreatic cancers, and nonsmall-cell lung carcinomas, are known to overexpress PD-L1, which allows cancer to evade the immune response by suppressing the adaptive immune system. The constitutive overexpression of PD-L1 on cancer cells reduces activation and proliferation of cancer-reactive T cells and induces T cells apoptosis. Consequently, disrupting the PD-1/PD-L1 complex at the cancer cell-T cell interface has become an attractive strategy of cancer immunotherapy and was awarded a Nobel Prize in Physiology or Medicine in 2018.[3] Immune checkpoint blockade-based therapies using monoclonal antibodies were shown potent in numerous clinical trials for patients with a broad spectrum of cancers, and these therapies delivered antitumor responses and long-term remissions.[4−9]

The global Checkpoint Inhibitors Market in 2018 was estimated to be almost $15 billion and predicted to grow to $26 billion by 2023.[10] It is solely based, though, on monoclonal antibodies (mAbs) with three PD-1 inhibitors (pembrolizumab, nivolumab, and cemiplimab) and three PD-L1 inhibitors (avelumab, atezolizumab, and durvalumab) approved by the U.S. Food and Drug Administration and The European Medicines Agency for various types of cancers, such as bladder, head and neck cancers, and kidney cancer, etc.[11,12] Additionally, there are over 1500 different clinical studies on PD-1/PD-L1 agents as of 2017, comprising mostly combination therapies with other targeted therapies and/or chemotherapy aiming at the discovery of synergistic effects. This clearly indicates how rapidly growing is the PD-1/PD-L1 immunotherapy market.[13]

Despite their proven efficacy, mAbs-based therapies are struggling with limitations including high treatment price, immune-related adverse events (irAEs), and poor tumor penetration related to their large size (150 kDa).[14,15] A way to overcome these shortcomings is presented with small-molecule-based therapeutics, which due to their size (usually below 0.5 kDa) would be orally bioavailable and cheaper in manufacturing while presenting improved pharmacokinetics and diffusion rates.[16] Even though there are plenty of patents regarding potent small-molecules targeted at PD-L1,[17−20] the only small molecule intended to target at PD-L1 currently in clinical trials is CA-170 from Curis and Aurigene, which is tested for the treatment of advanced solid tumors and lymphomas (NCT02812875, clinicaltrials.gov) and phase II clinical trials for lung cancer, head and neck/oral cavity cancer, MSI-H

Received: July 19, 2020
Published: September 16, 2020

positive cancers, and Hodgkin lymphoma in India (CTRI/2017/12/011026, ctri.nic.in). Three groups, including ours, have recently shown, however, that CA-170 is not a direct PD-L1-binder, which was evidenced in several independent biophysical and cell-based assays.[21−23]

The PD-1/PD-L1 interface is a challenging target due to its large, flat, and hydrophobic interface with a poorly defined binding pocket.[24] A popular way to approach such problematic targets is to use in silico screening further verified with a biophysical assay to eliminate false-positive "hits". However, to analyze the impact of chemical modifications on the inhibitor potency is nontrivial. One can predict how single changes will modify the chemical properties of the analyzed molecule, such as its solubility, hydrophobicity, etc., but we can only speculate how it will affect its interactions with the target protein. Therefore, an array of different modifications is usually applied to compare their influence on the final potency of the drug.

In the present study, we developed novel small-molecule inhibitors targeted at human PD-L1 that is potent in disrupting the PD-1/PD-L1 complex in biophysical and cell-based assays. To identify these inhibitors, we established a structure−activity relationship (SAR) screening cascade that is based on a new antagonist-induced dissociation assay nuclear magnetic resonance (NMR) screen, called weak-AIDA-NMR (w-AIDA-NMR).[25] w-AIDA-NMR facilitated the hit-to-lead design of the compounds capable of dissociating the preformed PD-1/PD-L1 complex. As compared to regular AIDA-NMR,[24,26,27] herein we used an N66A mutant of PD-1 that increases the K_d of the complex from 8 to ca. 100 μM, which hence allows small molecules, which are typically low-affinity binders, to be competitive in the complex formation. This was further followed by selectivity assays and structural biology directed medicinal chemistry design. The final compound **2k** was intended to be as small as possible and water-soluble, despite bearing two halogen atoms, while fulfilling other requirements from Lipinski's rule of five. In parallel, we perform in silico screening to guide the selection of the intermediate compounds.

RESULTS AND DISCUSSION

Identification of Fragments That Bind to PD-L1. The only small-molecule, nonpeptidic inhibitors, for which cocrystal structures with PD-L1 were reported, are based on a biphenyl core.[17,18,27] Because in silico design requires a high-resolution structure of the target, we used this common feature as a starting point for our SAR analysis. To find a seed fragment that could lead to the PD-L1 inhibitory compound, we conducted a w-AIDA-NMR screen on the available in-house library of decorated biphenyl compounds (data not shown). In parallel, we used a dimeric structure of PD-L1 with **BMS-1166** bound (PDB ID: 5NIX) for in silico screening with AutoDock Vina[28] integrated into PyRx software to identify plausible beneficial chemical modification.[29] From our in silico screening, we learned that a bromine, fluorine, or chlorine substitution decreased the binding affinity from −9.3 kcal/mol for 3-(bromomethyl)-1-1′-biphenyl to −9.8 kcal/mol, whereas hydroxyl and nitriles reduce the potency of the scaffold that indicates that the patch has to be hydrophobic. To validate the in silico predictions, we characterized selected compounds using the homogeneous time-resolved fluorescence (HTRF) assay (Figure 1). The IC_{50} values of **1a** and **1c** were determined to be around 51 and 56 μM, respectively, which is impressive for such small fragments with acceptable water solubility (Table S1). Moreover, the results of HTRF come in hand with our in silico

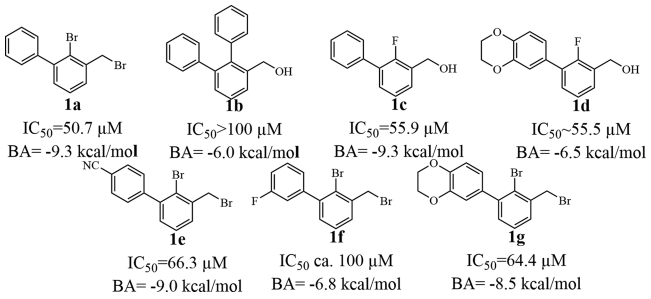

Figure 1. Comparison of selected short biphenyl-based initial scaffolds. BA stands for binding affinity.

screening where compounds **1a** and **1c** were the most prominent examples.

Because HTRF is prone to "false positives", especially aggregators and autofluorophores, we validated the results using the w-AIDA-NMR assay developed by us. In this assay, we introduced a mutation in the PD-1 binding pocket that effectively lowered its affinity toward PD-L1 so that short fragments could dissociate it. The mutation does not affect the PD-L1 binding interface to its inhibitors as described in detail in our methodology paper.[25] In the w-AIDA-NMR 2D experiment, ^{15}N mutated PD-1 gives a characteristic pattern of peaks (Figure 2A). Peak assignment is not necessary as we observe a relative change in the intensity and positions of the reference peaks upon the addition of ligand/inhibitors. Upon the formation of the complex with PD-L1, most of the cross-peaks in the ^{1}H−^{15}N HMQC spectrum of PD-1 became broader and less intense with some of the cross-peaks disappearing (Figure 2B). If the inhibitor is capable of disrupting the complex, the resulting spectrum should come back to the reference one of PD-1 alone, as tested inhibitors are PD-L1 binders. Out of the tested compounds, only bromine- and fluorine-substituted biphenyls (**1a** and **1c**) were capable of dissociating the mutant PD-1/PD-L1 complex at equimolar concentrations in the w-AIDA-NMR, which confirmed them not only to be binders but also putative seeds for lead inhibitory compounds as well (Figure 2C and D, respectively). Similar observations can be made using a 1D version of the w-AIDA-NMR, however, with nonlabeled, and hence cheaper to produce, protein. A characteristic aliphatic spectrum of PD-1 and PD-L1 is presented in Figure 2E, blue and red, respectively, with the most important PD-1 peaks highlighted with gray bars. Upon the complex formation (green curve), the highlighted peaks are flattened. However, after the addition of equimolar concentrations of **1a** and **1c**, those characteristic PD-1 peaks are restored indicating the dissociation of PD-L1 from the complex (purple and orange curves, respectively). Unambiguous identifications of short fragments potent to dissociate a PD-1/PD-L1 complex would not be possible using wild-type proteins, due to the too high binding constant between inhibitor and PD-L1 as presented in Figure S1.

Having the potential seed compounds identified, we continued with the second SAR step using in silico screening by designing the modification starting with the 2-bromo-3-(bromomethyl)-1,1′-biphenyl (calculated binding affinity of −10.2 kcal/mol). Because the biphenyl moiety is known to position resulting molecules within the cleft between the two PD-L1 units, we first decorated the phenoxymethyl with halogens and O-ether benzonitrile or the corresponding pyridine-cyanide to enhance the specificity of the binding by

https://dx.doi.org/10.1021/acs.jmedchem.0c01260
J. Med. Chem. 2020, 63, 11271−11285

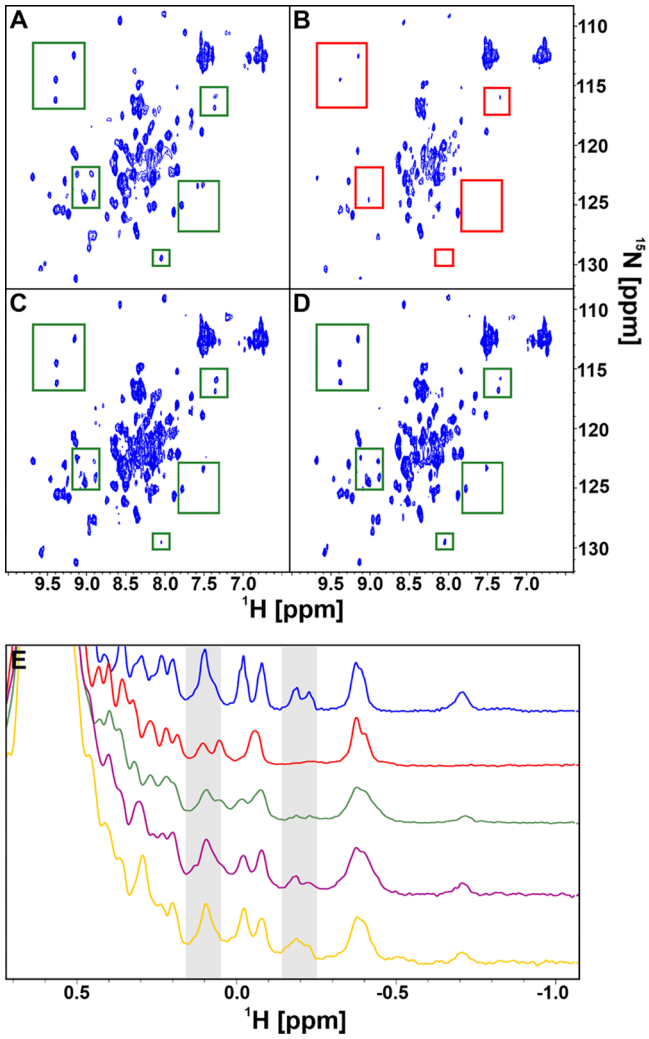

Figure 2. w-AIDA-NMR HSQC (A−D) and 1D NMR spectra (E). (A) N66A-PD-1 w-AIDA, five groups of characteristic peaks are boxed in green; (B) N66A-PD-1/PD-L1 complex, part of the PD-1 peaks disappeared, boxed in red; (C) N66A-PD-1/PD-L1 complex + **1a**, after addition of compound **1a** the spectrum of N66A-PD-1/PD-L1 complex resembles spectrum A; all PD-1 peaks are restored indicating the displacement of PD-L1 from the complex (peaks boxed in green); (D) N66A-PD-1/PD-L1 complex + **1c** spectrum resembles spectrum A; all PD-1 peaks are restored indicating the displacement of PD-L1 from the complex; (E) aliphatic part of the 1D NMR spectrum: blue, a characteristic spectrum of N66A-PD-1 is highlighted with gray bars; red, PD-L1spectrum, peaks in highlighted regions differ; green, spectrum of N66A-PD-1/PD-L1 complex, spectrum becomes flattened due to complex formation; purple, N66A-PD-1/PD-L1 complex + **1a**, restoration of characteristic PD-1 peaks due to addition of **1a** inhibitor; orange, N66A-PD-1/PD-L1 complex + **1c**, restoration of characteristic PD-1 peaks due to addition of **1c** inhibitor.

increasing the number of hydrogen donors/acceptors. To our surprise, we found two potent populations of compounds with the phenoxymethyl ring substituted with chlorine and O-ethers in the para position and bromine without ether substitution. As the last step, we tested various solubilizers to improve the water solubility of the scaffold, which would not decrease the potency, that resulted in final formulations of binding affinity between −10.5 and −11.5 kcal/mol.

After in silico identification of potential beneficial extension, we synthesized a group of compounds based on the 2-bromo-3-(bromomethyl)-1,1′-biphenyl moiety (**2a**−**k**) collected in Table 1. First, 2-bromo-3-(bromomethyl)-1,1′-biphenyl (**1a**) O-alkylation of various aldehydes in the presence of potassium carbonate was performed. Next, isolated aldehydes (**2a**−**d**) were subjected to the reductive amination mediated by sodium cyanoborohydride resulting in final structures (**2g**−**k**). In the case of compound **2f**, we performed a Williamson reaction between compound **1a** and methyl 3-bromo-4-hydroxybenzoate to isolate **2e** as the intermediate. We then introduced the amine component in the presence of DBU obtaining the final compound **2f**. All described compounds were tested in the HTRF assay to assess their biological activities as PD-1/PD-L1 complex inhibitors. Not surprisingly, the solubilities of the compounds heavily influence the resulting biological activities with aldehydes (**2a**−**d**) being substantially weaker than the corresponding scaffolds equipped with solubilizing groups (Table S1). The best results were obtained for compounds with a bromine at the R_1 position called from herein "di-bromo" with *N*-[2-(methylamino)ethyl]acetamide (**2g**) and pipecolic acid (**2k**) both exhibiting favorable low nanomolar IC_{50} values.

To extend the pool of functional groups, we tested a second generation of compounds based on 2-bromo-3-(bromomethyl)-1,1′-biphenyl (**1a**), [1,1′:2′,1″-terphenyl]-3′-ylmethanol (**1b**) resulting in compounds **3b**−**d**, **3f** (Table 2) and based on **1d** and **1e**−**g** fragments (Table 3). We included **1b**, **1d**, and **1e**−**g** fragments to further validate if initial screening using w-AIDA-NMR did not omit a potential hit. The synthesis started with the Mitsunobu reaction or the Williamson etherification of short fragment **1a** or **1b** with 5-chloro-2,4-dihydroxybenzaldehyde resulting in **3a** and **3e** intermediates. To prepare compounds **3b**,**c**,**f**, O-alkylation of phenolic aldehydes (**3a**, **3e**) with 4-(bromomethyl)picolinonitrile or 3-(bromomethyl)benzonitrile was carried out. The $NaBH_3CN$-mediated reductive amination was used to convert aldehyde **3b** into compound **3d**, but unexpectedly the product resulted to be unstable, without the possibility to isolate the pure compound (purity 64%). Similar reactions on other aldehyde substrates (**3a**, **c**, **e**, and **f**) were unsuccessful, which limited the possibility to compare the compounds' bioactivities. Clearly, the addition of bulky 4-(hydroxymethyl)pyridine-2-carbonitrile or 3-(hydroxymethyl)-benzonitrile at the position R_2 is favorable as they increase the number of hydrogen donors, however at the cost of the significantly higher molecular weight. Moreover, even though that structure of compound **3d** has already been disclosed in the patent WO2017202275A1 (example 3), the modifications that we did around it are not. Interestingly, our in silico screening routine failed to find more potent compounds reported in this patent, which proved that computational screening is still far from perfect and requires a thorough validation of the results with biophysical methods.

The preparation of inhibitors based on **1e**−**g** fragments comprised a synthetic pathway similar to that previously described. After the Williamson ether synthesis, a series of aldehydes (**4a**,**g**,**i**,**m**) or alcohol (**4m**) was isolated. The performance of sodium cyanoborohydride-mediated reductive amination with various amine components led to the conversion of aldehydes (**4a**,**g**,**i**,**m**) into final compounds (**4b**,**h**,**j**,**k**,**l**). To prepare the compound **4n**, the conversion of (3-((2-bromo-[1,1′-biphenyl]-3-yl)methoxy)phenyl)methanol (**4m**) to the corresponding chloride and a nucleophilic substitution with a thiomorpholine 1,1-dioxide was followed. Two other 1,1′:2′,1″-terphenyl- and 6-(2-fluorophenyl)-2,3-dihydrobenzo[*b*][1,4]-dioxine-based aldehydes (**4c**,**e**) were obtained by the potassium

https://dx.doi.org/10.1021/acs.jmedchem.0c01260
J. Med. Chem. 2020, 63, 11271−11285

Table 1. General Pathway for the Synthesis of Bromo Mono-Substituted Compounds[b]

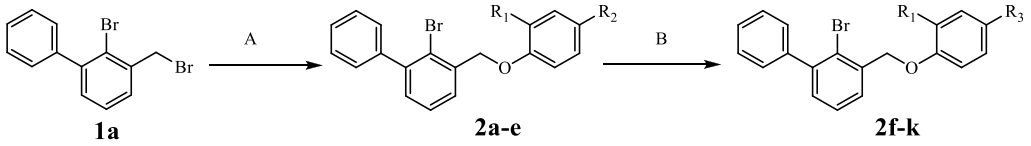

1a 2a-e 2f-k

A				B			
Name	R_1	R_2	IC_{50} [nM]	Name	R_1	R_3	IC_{50} [nM]
2a	-H		~50000	**2f**[a]	-Br	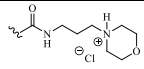	13200 ±150
2b	-Br		~50000	**2g**	-Br	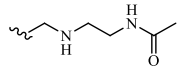	12.2 ±0.2
2c	-Me		~50000	**2h**	-H	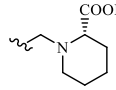	522.0 ±0.5
2d	-OMe		>100000	**2i**	-Me	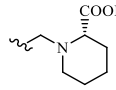	175.1 ±13.3
2e[a]	-Br		28 600 ±500	**2j**	-OMe	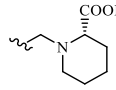	203.9 ±6.4
				2k	-Br	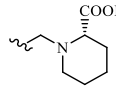	15.0 ±0.2

[a](A) Methyl 3-bromo-4-hydroxybenzoate, K_2CO_3, DMF, rt, overnight (45% for **2e**); (B) amine component R_3, DBU (25% for **2f**). [b]Reagents and conditions: (A) substituted 4-hydroxybenzaldehde, K_2CO_3, DMF, rt, overnight (43% for **2a**, 39% for **2b**, 38% for **2c**, and 52% for **2d**); (B) amine component, $NaBH_3CN$, AcOH, DMF, rt, overnight (53% for **2g**, 65% for **2h**, 56% for **2i**, 72% for **2j**, and 51% for **2k**).

carbonated promoted O-alkylation of 3-bromo-4-hydroxybenzaldehyde with **1b** and **1d** chlorides. The last step involved the $NaBH_3CN$-mediated reductive amination resulting in potential inhibitors **4d** and **4f**.

Because of the presence of two halogens and the solubilizer group, none of our best compounds passed Lipinski's rule of five, mainly due to the violation of mass and/or hydrophobicity requirements as calculated with the software Chemicalize (Table S1). However, the final compound **2k** showed the most promising overall parameters, being 90 Da smaller and with a 100 $Å^3$ van der Waals volume difference as compared to the second-best **3d**. Compounds **2k**, **2j**, and **2h** were additionally subjected to the competitive enzyme-linked immunosorbent assay (competitive ELISA) to compare their ability to dissociate human PD-1/PD-L1 complex as compared to **BMS-1166** (a potent PD-1/PD-L1 inhibitor from Bristol-Myers Squibb Co.) (Figure S2). According to the results, compound **2k** is a stronger inhibitor as compared to **BMS-1166** (1.47 ± 0.05 and 28.04 ± 0.36 nM, respectively), which further proved the potency of our final product.

NMR-Binding Assay. The direct binding of the most prominent compounds **2k** and **3d** to the human PD-L1 was also confirmed with a ^1H NMR method (Figure S3). In the assay, the addition of the tested molecules **2k** and **3d** caused a characteristic dimerization of hPD-L1 that we observed for the biphenyl compounds previously,[27] evidenced by the broadening of the NMR peaks in the aliphatic region of the ^1H NMR spectrum as compared to the NMR spectrum of the apo hPD-L1.

Cell-Based Assay. The most prominent compounds from HTRF assay were tested in the PD-1/PD-L1 immune checkpoint blockade cell-based assay. In the assay, the PD-1/PD-L1 interaction is provided by the cocultured artificial antigen-presenting cells (aAPCs) and Jurkat reporter T cells. The compounds that disrupt this interaction increase a TCR-mediated activation of the Jurkat cells, evidenced by the increased activity of luciferase. The luciferase activity thus reflects the activation status of the Jurkat T cells.

Durvalumab, a clinically relevant PD-L1-blocking antibody, released the TCR signaling with the EC_{50} value of 0.2 ± 0.06 nM, as revealed by the fitting of Hill's equation to the experimental data set (Figure 3). All of the tested compounds were also able to increase the activation of the effector cells, but at considerably higher concentration ranges than durvalumab. For Hill's equation fitting, the maximal response to durvalumab was set as a maximum allowed activation of the Jurkat effector cells, because for the other compounds the activation plateau could not be reached. Out of the tested compounds, compound **2k** provided the highest level of the Jurkat T cell activation (2.1-fold at a 50 μM concentration of a compound in the assay) and

https://dx.doi.org/10.1021/acs.jmedchem.0c01260
J. Med. Chem. 2020, 63, 11271−11285

Table 2. General Pathway for the Synthesis of Extended 2-Bromo-3-(bromomethyl)-1,1′-biphenyl (1a) and [1,1′:2′,1″-Terphenyl]-3′-ylmethanol (1b)-Based Compounds 3b−d, 3f[a]

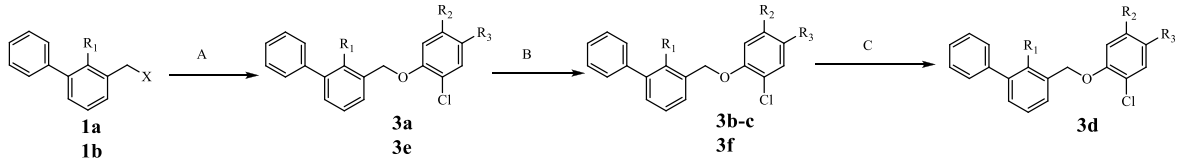

Name	R_1	R_2	R_3	IC_{50} [nM]
3a	-Br	-OH		>100000
3b	-Br	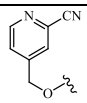		29400 ±450
3c	-Br			551.9 ±13.2
3d	-Br	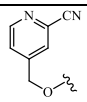	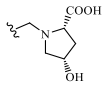	3.9 ±0.1
3e	-Ph	-OH		>100000
3f	-Ph	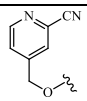		23800 ±130

[a]Reagents and conditions: (A) for compound **1a** where X is −Br, 5-chloro-2,4-dihydroxybenzaldehyde, $NaHCO_3$, ACN/DMF, rt, overnight (54% for **3a**); for compound **1b** where X is −OH, 5-chloro-2,4-dihydroxybenzaldehyde, PPh_3, DIAD, THF, rt, overnight (20% for **3e**); (B) picolinonitrile/benzonitrile component, K_2CO_3, DMF, rt, overnight (63% for **3b**, 87% for **3c**, and 90% for **3f**); (C) amine component, $NaBH_3CN$, AcOH, DMF, rt, overnight (for **3d**).

the lowest EC_{50} value of 6.6 ± 0.8 μM (Figure 3). This activation was much better than the activation observed for the patented compound **3d** (EC_{50} value of 12.2 ± 1.4 μM), for which solubility problems in DMSO/water conditions were observed, which disallowed data collection for the two highest concentrations. Compound **2g** showed activity similar to that of **2k** (EC_{50} value of 6.8 ± 1.1 μM). However, due to the toxicity of the compound **2g**, observed above 10 μM concentration, the value had to be estimated on the basis of partial data. Other compounds exhibit EC_{50} > 40 μM and low activation levels.

The final compound **2k** was also found not to be toxic up to 100 μM final concentration in cell viability assay (Figure S4). As compared to the BMS compounds tested in Skalniak et al. (2017), Figure 2a,[27] this is a significantly better result, as the potent **BMS-1166** decreased the viability of the cells by 50% at 40 μM concentration, while it decreased the viability of other BMS compounds at even lower inhibitor concentrations.

The biological activity of the compound **2k** was further verified on the primary T cells. For this, peripheral blood mononuclear cells (PBMCs) isolated from the blood of healthy donors were contacted with hPD-L1 aAPCs to provide TCR-mediated activation of T cells and the engagement of PD-1/PD-L1 immune checkpoint. The cells were then analyzed with flow cytometry following the gating for $CD4^+$ and $CD8^+$ T cells. The blockade of the PD-1/PD-L1 immune checkpoint was expected to increase the activation of T cells. In the experiment, atezolizumab and compound **2k** were used. Neither of the two molecules was able to increase the expression of an early T-cell activation marker, CD69 (not shown). Because the prolonged activation of T cells leads to the increase of the expression of immune checkpoint molecules,[30] we have monitored the expression of PD-1 protein itself as an indicator of the late T cell activation and exhaustion. In fact, the treatment with both the control antibody atezolizumab and the compound **2k** led to a significant increase of the expression of PD-1 receptor on the surface of both $CD4^+$ and $CD8^+$ T cells (Figure 4). This confirms the bioactivity of the compound **2k** in the context of primary T cells.

Cross-Reactivity of the PD-L1/PD-1-Blocking Small Molecules for Human and Murine PD-L1. Several compounds based on the biphenyl core were subjected to the MicroScale Thermophoresis (MST) experiment to determine their cross-reactivity toward murine and human PD-L1's. We used both the human (for the positive control) and the murine PD-L1 for **2k**, **2i**, **2g**, and **BMS-1166**, and the murine anti-PD-L1 antibody MIH-5 as the positive control for murine PD-L1

https://dx.doi.org/10.1021/acs.jmedchem.0c01260
J. Med. Chem. 2020, 63, 11271−11285

Table 3. General Pathway for the Synthesis of 6-(2-Bromo-3-(bromomethyl)phenyl)-2,3-dihydrobenzo[*b*][1,4]dioxine (1g), 1,1′:2′,1″-Terphenyl (1b), 6-(3-(Bromomethyl)-2-fluorophenyl)-2,3-dihydrobenzo[*b*][1,4]dioxine (1d), [1,1′:2′,1″-Terphenyl]-3′-ylmethanol, 2-Bromo-3-(bromomethyl)-3′-fluoro-1,1′-biphenyl (1f), and 2′-Bromo-3′-(bromomethyl)-[1,1′-biphenyl]-4-carbonitrile (1e)-Based Compounds 4a−n[a]

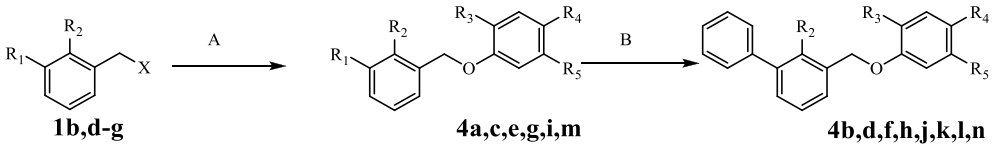

	R_1	R_2	R_3	R_4	R_5	IC_{50} [nM]
4a	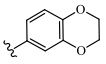	-Br	-Br		-H	35400 ±300
4b	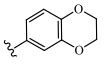	-Br	-Br	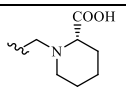	-H	401.0 ±2.1
4c	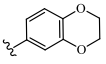	-F	-Br		-H	>100000
4d	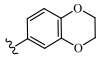	-F	-Br	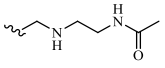	-H	22.7 ±1.0
4e	-Ph	-Ph	-Br		-H	>100000
4f	-Ph	-Ph	-Br	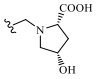	-H	29400 ±450
4g	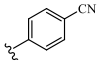	-Br	-Br		-H	>100000
4h	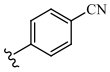	-Br	-Br	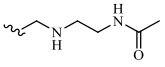	-H	5114 ±58
4i	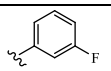	-Br	-Br		-H	~55000
4j	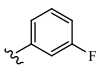	-Br	-Br	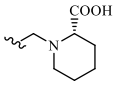	-H	65.3 ±0.7
4k	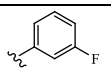	-Br	-Br	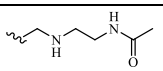	-H	106.8 ±20.8
4l	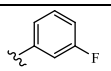	-Br	-Br	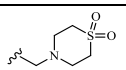	-H	4238 ±86
4m	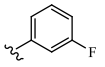	-Br	-H	-H		>100000
4n	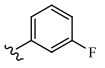	-Br	-H	-H	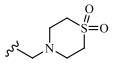	22300 ±230

[a]Reagents and conditions: (A) for compounds **1e−g** where X is −Br, substituted 4-hydroxybenzaldehde, K_2CO_3, DMF, rt, overnight (88% for **4a**, 61% for **4g**, 57% for **4i**, and 52% for **4m**); for compounds **1b**, **1d** where X is −OH, (1) $SOCl_2$, DCM, 40 °C, (2) substituted 4-hydroxybenzaldehde, K_2CO_3, DMF, rt, overnight (30% for **4c** and 60% for **4e**); (B) for compounds **4a,c,e,g,i**, amine component, $NaBH_3CN$, AcOH, DMF, rt, overnight (43% for **4b**, 61% for **4d**, 37% for **4f**, 26% for **4h**, 44% for **4j**, 67% for **4k**, and 33% for **4l**); for compounds **4m**, (1) $SOCl_2$, DCM, 40 °C, (2) amine component, K_2CO_3, DMF, rt, overnight (29% for **4n**).

https://dx.doi.org/10.1021/acs.jmedchem.0c01260
J. Med. Chem. 2020, 63, 11271−11285

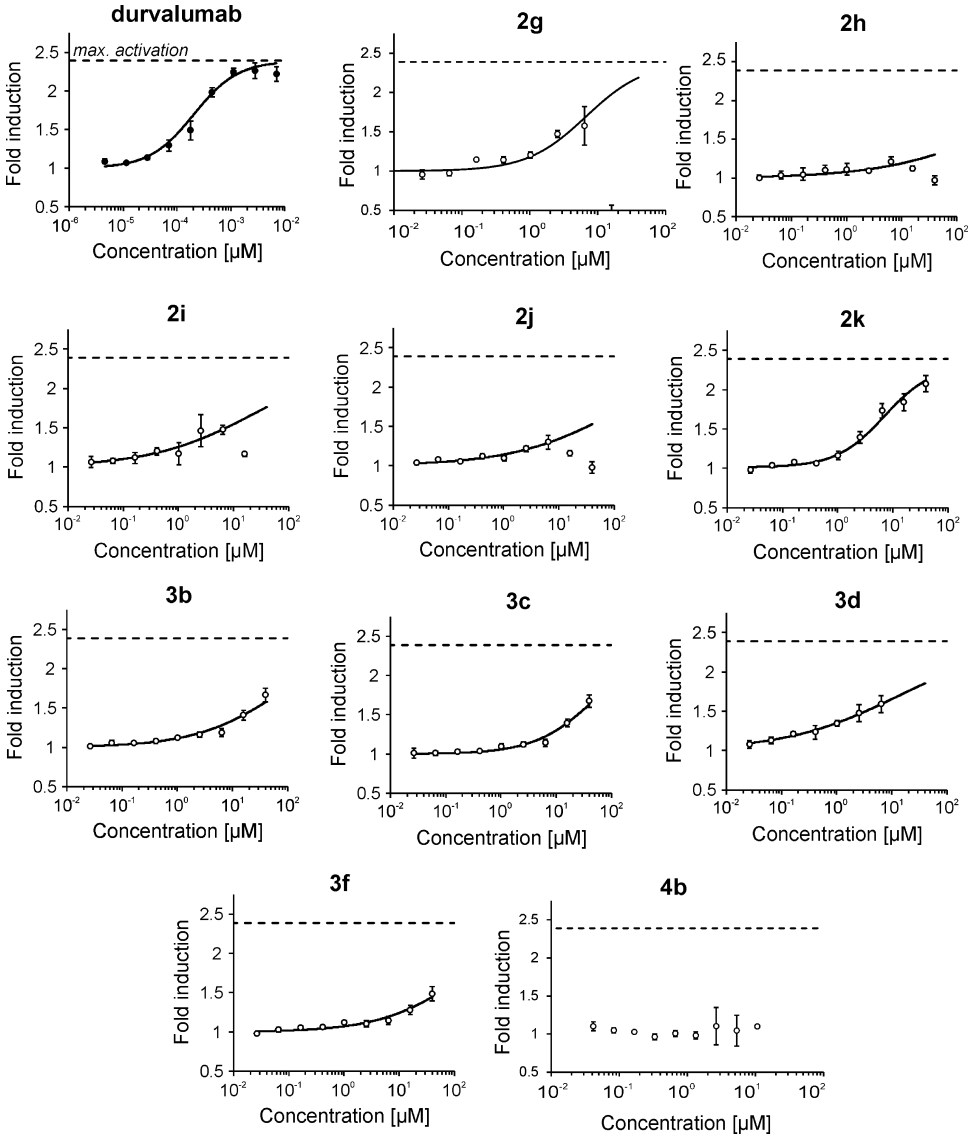

Figure 3. Activity of modified bromo compounds in PD-1/PD-L1 immune checkpoint blockade cell-based assay. Activities of the reference anti-PD-L1 antibody durvalumab and tested compounds in alleviating the effect of PD-1/PD-L1 checkpoint on TCR-mediated effector Jurkat T cells are expressed as fold induction of the luciferase activity, the expression of which is TCR-inducible (for details, please see the Experimental Section). The graphs present relative luminescence normalized to DMSO-treated controls and are mean ± SEM values from 4 to 7 independent experiments.

(Figure S5A–E, respectively). The experiment showed that the compounds based on the biphenyl moiety were not active against the murine PD-L1, as they did not cause any changes in the fluorescence spectrum upon addition to the protein solution, whereas they have a clear pattern when tested against the human PD-L1, with **2k** and **2g** being the tighter binders (dissociation constants K_D of 4.0 and 3.2 nM, respectively) than **BMS-1166** (K_D of 30.3 nM) (Table S2). This MST result disqualifies the biphenyl-based compounds for the experiments on the syngeneic mice as there is no cross-reactivity between human and murine targets.

Modeled Interactions with Dimeric PD-L1. To explore the molecular interactions of most potent compounds **2k** and **3d** with PD-L1, we docked the compounds into a dimeric PD-L1 using the PyRx software. To refine the docking results, residues interacting with those compounds were allowed flexibility in their side chains. The interactions then were assessed using the Protein–Ligand Interaction Profiler (Figure 5).[31] The core of the scaffold for both molecules is the same, with the biphenyl structure positioning the molecules with its strong and conserved stabilizing $\pi-\pi$ stacking with Tyr56A and an aromatic phenyl ring with Tyr56B. The hydrogen bonding of **2k** comes from the interactions between the Tyr56B hydroxyl group and nitrogen atom from the pipecolic acid moiety and Asn63B amide nitrogen and oxygen from the carboxylic group of a solubilizer. For **3d**, hydrogen bonds are predicted between cyanopyridine nitrogen with Arg125A nitrogen and nitrile group nitrogen with Asn63B nitrogen. Clever usage of solubilizer in **2k** allows for a great reduction in molecule size by 90 Da, down to 557 Da (close to the Lipinski's size rule requirement <500 Da). Moreover, the tertiary amine in solubilizers of both **3d** and **2k** is predicted to be involved in salt bridges with the Asp122A negatively charged carboxyl group stabilizing the whole complex. Both compounds are also involved in several hydrophobic interactions with residues Ile54A Tyr56A and B, Gln66B, Met115B, and either Ala121A for **2k** or Ala121B for **3d**, as well as Tyr123A that comes from the main scaffold (**2a**).

https://dx.doi.org/10.1021/acs.jmedchem.0c01260
J. Med. Chem. 2020, 63, 11271–11285

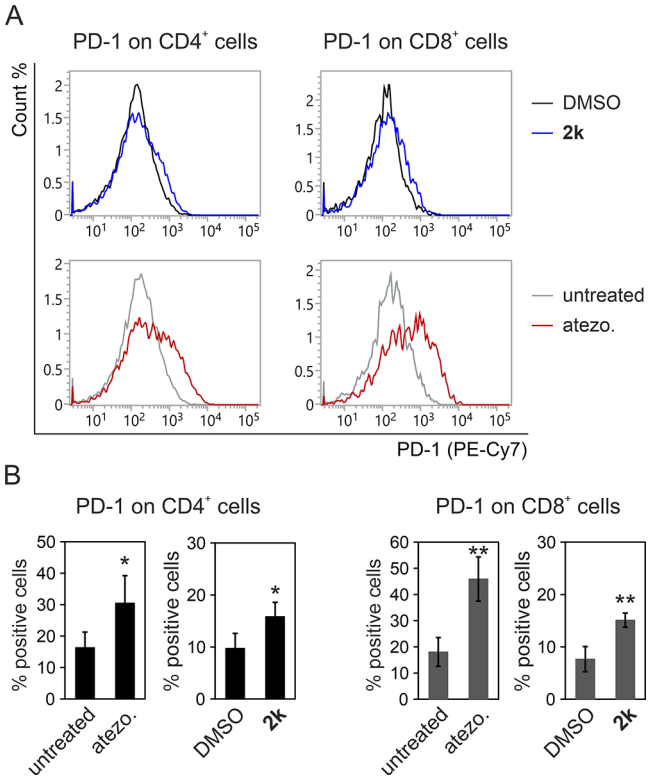

Figure 4. Compound **2k** blocks the PD-L1/PD-1 immune checkpoint in primary human T cells, as evidenced by the increased expression of the late activation and exhaustion marker, PD-1. Peripheral blood mononuclear cells (PBMCs) were seeded on the preseeded hPD-L1 aAPCs and cultured for 48 h alone or in the presence of **2k**, DMSO (as a solvent for **2k**), or atezolizumab (atezo., an anti-PD-L1 therapeutic antibody). The expression of PD-1 was tested with flow cytometry. (A) Exemplary histograms, presenting the increased expression of PD-1 on either the CD4+ or the CD8+ T cells. (B) The analysis of the expression of PD-1 on CD4+ or CD8+ T cells under control conditions and in the presence of PD-L1-blocking molecules, the antibody atezolizumab, and compound **2k**. Graphs present mean ± SD values calculated for three independent experiments performed with the engagement of different donors. Statistical significance was analyzed with the Student's *t* test: $*p < 0.05$, $**p < 0.01$.

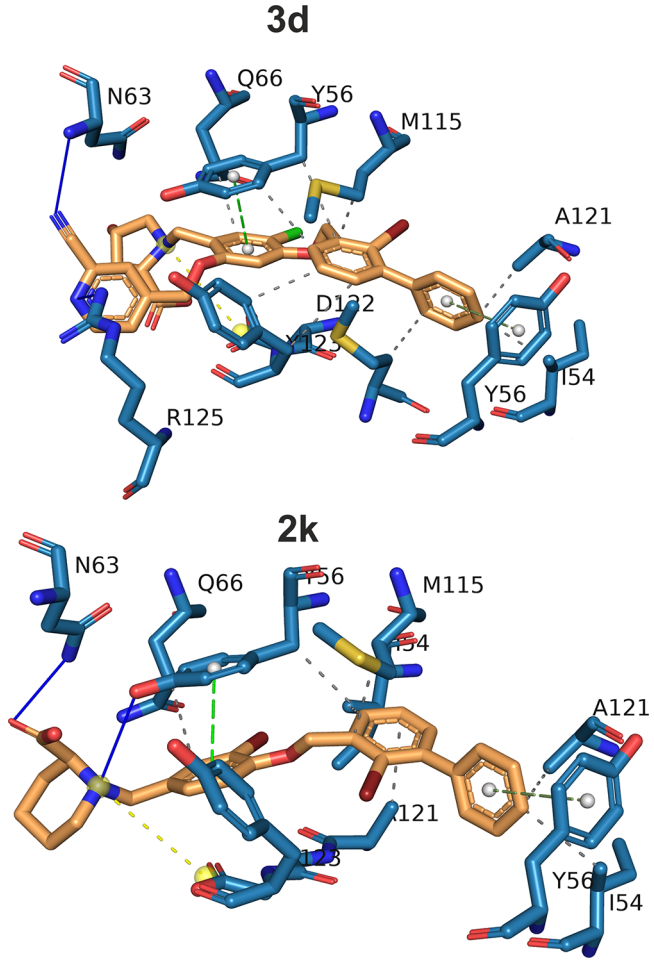

Figure 5. Interactions between PD-L1 and **3b** (top) and **2k** (bottom) from modeled complexes (compounds were docked on PD-L1 taken from PDB ID: 5NIX). Both compounds are involved in a number of hydrophobic interactions (gray dashed lines) with residues Ile54A Tyr56A and B, Gln66B, Met115B, Ala121A for **3b** and Ala121B for **2h**, and Tyr123A. There is strong conserved stabilizing π-stacking (green dashed line) between the distal phenyl ring from the biphenyl moiety and Tyr56A and the phenyl from phenoxymethyl with Tyr56B. The major differences are in the hydrogen bonds (blue solid line), which for **2k** are between the Tyr56B hydroxyl group and the tertiary amine in piperidine solubilizer and the Asn63B amide nitrogen and oxygen from the carboxylic group of the solubilizer. For **3b**, hydrogen bonds are between the cyanopyridine nitrogen with Arg125A nitrogen and the nitrile group nitrogen with Asn63B nitrogen.

CONCLUSIONS

Herein, we demonstrate a new, potent compound that can dissociate the PD-1/PD-L1 complex, with the potency of inciting adaptive immune system and activating cancer-reactive T cells. Our final compound **2k** is significantly smaller than other small-molecule inhibitors reported in the literature. The design process was based on the novel methodology for the identification of potent small-molecular fragments, with w-AIDA-NMR as the starting block for further extensions. Tested fragments were not able to dissociate the native PD-1/PD-L1 complex in AIDA-NMR (Figure S1), which proved the usefulness of w-AIDA-NMR in the identification of small potent fragments for inhibitors. w-AIDA-NMR offers unambiguity of the results, due to the simplest system possible, protein and compound in the buffer of your choice, and ensures that the core fragment is capable of dissociating the complex. Moreover, using this technique, one can instantly spot compounds that are precipitating or aggregating the target protein as well as controlling the solubility of the tested fragment, a common issue in other biophysical assays. Because it is not based on the modification of light, it will not generate "false positives", significantly reducing time and cost commitment in developing "falsified hits". Each intermediate step was validated with the HTRF affinity determination and later with the cell-based assay. The final compound **2k** was shown to be more potent than other molecules tested here and able to activate Jurkat cells to a degree close to that of the control antibody. In fact, **2k** is the strongest small-molecule inhibitor of PD-L1 reported in the literature including potent **BMS-1166** and **BMS-1001**.[27] Thanks to its enhanced solubility and small size, **2k** is neutral to cell viability even at a 100 μM concentration. Because of the lack of cross-reactivity between human and murine PD-L1 for biphenyl-based compounds, we were not able to perform experiments on mice. However, we were able to prove the bioactivity of the compound **2k** in the experiments with primary T cells isolated from the blood of healthy donors by monitoring the expression of PD-1 receptor on the surface of both $CD4^+$ and $CD8^+$ T cells.

https://dx.doi.org/10.1021/acs.jmedchem.0c01260
J. Med. Chem. 2020, 63, 11271−11285

EXPERIMENTAL SECTION

Protein Expression and Purification. All chemicals used for protein expression and purification were purchased from BioShop (Bioshop Canada Inc., Burlington, ON, Canada) and Sigma-Aldrich (Sigma-Aldrich Corporation, St. Louis, MO) and were used without any additional purification. The IgV domains of human and mouse PD-L1 protein (hPD-L1 residues, 18−134, C-terminal His-tag; mPD-L1 residues, 19−134) and the extracellular domain of human PD-1 (hPD-1 residues 34−150, C93S) were expressed and purified as described previously.[24] Proteins were expressed in the *Escherichia coli* BL21 (DE3). Bacterial cells were cultured at 37 °C in LB or M9 minimal medium containing $^{15}NH_4Cl$ as the sole nitrogen source to achieve ^{15}N isotope labeling. Proteins expression was induced with 1 mM osopropyl β-D-1-thiogalactopyranosid (IPTG) at an OD_{600} of 0.8, and the cells were cultured overnight. For hPD-1, the temperature was lowered to 28 °C. The inclusion bodies purification was carried out as described previously.[32] Afterward proteins were refolded by dropwise dilution into a solution containing 0.1 M Tris pH 8.0, 0.4 M L-arginine hydrochloride, 2 mM EDTA, 5 mM cystamine, and 0.5 mM cysteamine for hPD-1, and 0.1 M Tris pH 8.0, 1 M L-arginine hydrochloride, 0.25 mM oxidized glutathione, and 0.25 mM reduced glutathione for hPD-L1. After refolding, proteins were dialyzed three times against solution containing 10 mM Tris pH 8.0 and 20 mM NaCl. Finally, proteins were purified by SEC (size-exclusion chromatography) on an HiLoad 26/600 Superdex 75 column (GE Healthcare, Chicago, IL) in 25 mM sodium phosphate pH 6.4 with 100 mM NaCl for hPD-1, N66A hPD-1 mutant or in PBS pH 7.4 for hPD-L1, hPD-L1(18−239).

AIDA-NMR. Uniform ^{15}N labeling was obtained by expressing proteins in the M9 minimal medium containing $^{15}NH_4Cl$ as the sole nitrogen source. 10% (v/v) of D_2O was added to the samples to provide the lock signal. All spectra were recorded at 300 K using a Bruker Avance III 600 MHz spectrometer equipped with the nitrogen cryoprobe. The ability of tested compounds to dissociate PD-L1/(wild type, wt or N66A)PD-1 was evaluated using the (weak) antagonist-induced dissociation assay (w-AIDA-NMR). In brief, ^{15}N-labeled wt- and N66A PD-1 (0.15 mM) were slightly overtitrated with the unlabeled PD-L1. The compounds were aliquoted into the resulting mixture. During the experiment, the $^1H-^{15}N$ signals were monitored by SOFAST HMQC.

Homogeneous Time-Resolved Fluorescence. The HTRF assay was performed using the certified Cis-Bio assay kit at 20 μL final volume using their standard protocol (5 nM of hPD-L1 and 50 nM of hPD-1 in the final formulation). To determine the half maximal inhibitory concentration (IC_{50}) of the tested compounds, measurements were performed on individual dilution series. After all components were mixed according to Cis-Bio protocol, the plate was left for 2 h incubation at room temperature followed by TR-FRET measurement on a Tecan Spark 20M. Collected data were background subtracted on the negative control, normalized on the positive control, averaged, and fitted with a normalized Hill's equation to determine the IC_{50} value using Mathematica 12.

Cell Culture. CHO K-1 cells overexpressing hPD-L1 and the recombinant TCR ligand (hPD-L1 Antigen Presenting Cells, hPD-L1 aAPCs) (Promega, Madison, WI) and Jurkat T cells overexpressing hPD-1 and carrying a luciferase reporter gene under the control of Nuclear Factor of Activated T-cells Response Element (NFAT-RE) (hPD-1 Effector Cells, hPD-1 ECs, Promega) were cultured in RPMI-1640 medium (Biowest, Billerica, MA) supplemented with 10% Fetal Bovine Serum (FBS, Biowest) and 200 mM L-glutamine (Biowest) in the presence of G418 (250 μg/mL, InvivoGen, San Diego, CA) and Hygromycin B Gold (50 μg/mL, InvivoGen) as selection antibiotics. The overexpression of hPD-L1 and TCR ligand in aAPCs and PD-1 in ECs was confirmed by flow cytometry and Western blot analysis, respectively. PCR tests for *Mycoplasma* sp. contamination[33] were routinely performed and indicated negative results for both cell lines.

hPD-1/hPD-L1 Immune Checkpoint Blockade Assay. The activity of the inhibitors of the hPD-1/hPD-L1 immune checkpoint was examined using the hPD-1/hPD-L1 Blockade Bioassay (Promega), according to the manufacturer's instructions. hPD-L1 aAPCs were seeded on 96-well (white) plates at the density 10 000 cells/well 17 h prior to the experiment. The 2.5-fold dilution of the small molecules was first prepared in DMSO. On the day of the assay, the compounds were diluted 1000-fold in the assay buffer (99% RPMI 1640, 1% FBS) to maintain the constant concentration of DMSO (0.1% of total volume). The 2.5-fold dilutions of durvalumab, a positive control anti-hPD-L1 monoclonal antibody (Imfinzi, Medimmune/AstraZeneca), were prepared in the assay buffer on the day of the assay. The culture medium was discarded from the wells, and serial dilutions of either the small molecule or the antibody were added. Afterward, Jurkat hPD-1 cells were seeded at the density of 20 000 cells per well in the assay's plates. After 6 h of incubation in standard culture conditions, assay plates were equilibrated at ambient temperature for 10 min, followed by a 20 min incubation with the Bio-GloTM Assay reagent (Promega). The luminescence was detected using the Spark microplate reader (Tecan). Half maximal effective concentrations (EC_{50} values) were calculated from Hill's curve fitting to the experimental data.

Isolation of Peripheral Blood Mononuclear Cells (PBMCs). Blood samples from healthy donors were purchased from the Regional Center of Blood Donation and Blood Therapy in Krakow. PBMCs were isolated by a density gradient centrifugation using Pancoll human separating solutions (PAN-Biotech) and then resuspended in RPMI 1640 medium (Biowest) containing 10% FBS (Biowest).

Flow Cytometry Analysis of Activation Markers. PBMCs were added to the preseeded aAPCs at the density of 400 000 cells/well and incubated in the presence of compound **2k**, DMSO, and with or without atezolizumab (5 μg/mL) as an anti-PD-L1 monoclonal antibody. After 48 h, cells were detached using TrypLe Select Enzyme (Thermo Fisher Scientific), collected into 5 mL round-bottom tubes, and washed with flow cytometry staining buffer (Thermo Fisher Scientific). For flow cytometry analysis, cells were stained using monoclonal antibodies: anti-CD69-APC, anti-CD4-FITC, anti-CD8-BV510, and anti-PD1-PECy7 (Becton Dickinson, BD). Following 20 min of incubation at room temperature, cells were washed, resuspended in PBS, and analyzed using a FACSCanto II flow cytometer (BD) and FACSDiva software (BD). The data analysis was carried out with FACSuite software (BD).

Molecular Docking and In Silico Screening. The compounds were generated as a permutation of all (interesting to us) functional groups on biphenyl scaffold (over 1500 structures), which were then minimized using OpenBabel software. For molecular docking of putative inhibitors, we used AutoDock Vina[28] integrated into PyRx with the dimeric structure of PD-L1 with **BMS-1166** bound (PDB ID: 5NIX). On the basis of the scoring results and feasibility of chemical synthesis, we selected the most interesting compounds.

Chemical Synthesis of Compounds. *General Information.* Starting materials and solvents were received from Sigma-Aldrich, Cool Pharm, Idalia, and Alfa Aesar, and they were used without additional purification. ^1H and ^{13}C NMR spectra were recorded on a Bruker Avance 600 MHz spectrometer with a report of chemical shifts (δ) in ppm and coupling constants (J) in Hz. TMS was used as the reference and an internal standard with a singlet at δ 0 ppm. Moreover, chemical shifts were analyzed in correspondence to the solvent peaks (DMSO-d_6, $CDCl_3$).

Infrared spectra were recorded for the solid samples on a Nicolet IR200 spectrometer due to the ATR technique. High-resolution mass spectrometry (HRMS) analysis was performed on a microTOF-QII apparatus using the ESI ionization mode. Purification of compounds was conducted thanks to flash chromatography on the Grace Reveleris X2 Flash Chromatography System with Grace Resolv Silica Cartridges. The UPLC−MSs were recorded on the TQD Waters H-Class spectrometer (column, ACQUITY UPLC BEH C18 1.7 um, 2.1 × 50 mm; method, 6 min; gradient, 0−3 min 80% H_2O−20% MeCN, 3−3.5 min 100% MeCN, 3.5−6 min 80% H_2O−20% MeCN). All final compounds were determined to have at least 95% purity. Thin-layer chromatography (TLC) was performed thanks to use of aluminum sheets precoated Silica Gel 60 F_{254} (Merck). Techniques of visualization of TLC plates included using an UV lamp with radiation at 254 nm wavelength. Melting points were determined with an Ascon-M5 apparatus.

https://dx.doi.org/10.1021/acs.jmedchem.0c01260
J. Med. Chem. 2020, 63, 11271−11285

The syntheses of substrates and the preparation of short fragments **1a**−**1g** are described in the Supporting Information.

*4-((2-Bromo-[1,1′-biphenyl]-3-yl)methoxy)benzaldehyde (**2a**).* **1a** (200 mg, 0.62 mmol), 4-hydroxybenzaldehyde (75 mg, 0.62 mmol), and potassium carbonate (170 mg, 1.23 mmol) were stirred in anhydrous DMF (3 mL) at room temperature overnight. The solvent was removed under reduced pressure. Water was added (30 mL), and the mixture was extracted with AcOEt (2 × 30 mL). Organic layers were combined and concentrated. Crude product was purified by column chromatography on silica gel (0−100% AcOEt in hexane) and crystallized from cyclohexane to yield **2a** (97 mg, 43%) as a white solid. ^{1}H NMR (600 MHz, $CDCl_3$) δ: 9.91 (s, 1H), 7.90−7.86 (m, 2H), 7.54−7.51 (m, 1H), 7.47−7.37 (m, 6H), 7.31 (dd, J = 7.5, 1.7 Hz, 1H), 7.15−7.12 (m, 2H), 5.30 (s, 2H). ^{13}C NMR (151 MHz, $CDCl_3$) δ: 190.8, 163.4, 143.7, 141.1, 136.1, 132.1, 130.9, 130.4, 129.4, 128.1, 127.8, 127.5, 127.4, 122.6, 115.2, 70.4. IR (ATR): 2916, 2849, 2835, 1684, 1598, 1591 1508, 1422, 1260, 1164, 1046 cm^{-1}. HRMS ESI−MS-q-TOF for $C_{20}H_{15}BrO_2$ $[M + Na]^+$ found, 389.0148 m/z; calcd mass, 389.0153. Mp: 87.7 °C. UPLC−MS (DAD/ESI): t_R = 8.78 min, for $C_{20}H_{15}BrO_2$ $[M + H]^+$ found, 367.18 m/z; calcd mass, 367.03.

*3-Bromo-4-((2-bromo-[1,1′-biphenyl]-3-yl)methoxy)-benzaldehyde (**2b**).* Compound **2b** was prepared following the procedure for **2a**. Preparation involved the use of **1a** (220 mg, 0.68 mmol), 3-bromo-4-hydroxybenzaldehyde (136 mg, 0.68 mmol), and potassium carbonate (187 mg, 1.36 mmol), which were stirred in anhydrous DMF (3 mL) at room temperature overnight. Crude product was purified by column chromatography on silica gel (0−100% AcOEt in hexane) and yielded **2b** (119 mg, 39%) as a white solid. ^{1}H NMR (600 MHz, $CDCl_3$) δ: 9.87 (s, 1H), 8.15 (d, J = 2.0 Hz, 1H), 7.83 (dd, J = 8.4, 2.0 Hz, 1H), 7.69 (d, J = 7.7 Hz, 1H), 7.49−7.37 (m, 6H), 7.32 (dd, J = 7.5, 1.5 Hz, 1H), 7.11 (d, J = 8.5 Hz, 1H), 5.36 (s, 2H). ^{13}C NMR (151 MHz, $CDCl_3$) δ: 189.7, 159.5, 143.6, 141.1, 135.7, 134.8, 131.3, 131.3, 130.9, 129.6, 128.2, 127.9, 127.7, 127.2, 121.9, 113.4, 113.1, 71.1. IR (ATR): 3082, 2923, 2852, 1683, 1593, 1492, 1276, 1256, 1185, 1050 cm^{-1}. HRMS ESI−MS-q-TOF for $C_{20}H_{14}Br_2O_2$ $[M + Na]^+$ found, 466.9249 m/z; calcd mass, 466.9258. Mp: 151.2 °C. UPLC−MS (DAD/ESI): t_R = 9.37 min, for $C_{20}H_{14}Br_2O_2$ $[M + H]^+$ found, 447.07 m/z; calcd mass, 446.94.

*4-((2-Bromo-[1,1′-biphenyl]-3-yl)methoxy)-3-methylbenzaldehyde (**2c**).* Compound **2c** was obtained according to the procedure of **2a**, using **1a** (200 mg, 0.62 mmol), 4-hydroxy-3-methylbenzaldehyde (84 mg, 0.62 mmol), potassium carbonate (170 mg, 1.23 mmol), and anhydrous DMF (3 mL). Crude product was purified by column chromatography on silica gel (0−100% AcOEt in hexane) and was crystallized from cyclohexane to yield **2c** (90 mg, 38%) as a white solid. ^{1}H NMR (600 MHz, $CDCl_3$) δ: 9.88 (s, 1H), 7.76 (d, J = 1.1 Hz, 1H), 7.73 (dd, J = 8.3, 2.0 Hz, 1H), 7.57−7.53 (m, 1H), 7.47−7.38 (m, 6H), 7.32 (dd, J = 7.5, 1.7 Hz, 1H), 7.03 (d, J = 8.4 Hz, 1H), 5.30 (s, 2H), 2.41 (s, 3H). ^{13}C NMR (151 MHz, $CDCl_3$) δ: 191.3, 161.7, 143.7, 141.3, 136.6, 131.8, 130.8, 130.1, 129.6, 128.2, 128.1, 127.9, 127.5, 127.3, 122.5, 111.2, 70.4, 16.7. IR (ATR): 2821, 1679, 1599, 1260, 1240, 1125, cm^{-1}. HRMS ESI−MS-q-TOF for $C_{21}H_{17}BrO_2$ $[M + Na]^+$ found, 403.0304 m/z; calcd mass, 403.0309. Mp: 144.5 °C. UPLC−MS (DAD/ESI): t_R = 9.31 min, for $C_{21}H_{17}BrO_2$ $[M + H]^+$ found, 381.20 m/z; calcd mass, 381.05.

*4-((2-Bromo-[1,1′-biphenyl]-3-yl)methoxy)-3-methoxybenzaldehyde (**2d**).* Compound **2d** was prepared following the procedure for **2a**. Preparation involved the use of **1a** (300 mg, 0.93 mmol), 4-hydroxy-3-methoxybenzaldehyde (141 mg, 0.93 mmol), and potassium carbonate (255 mg, 1.85 mmol), which were stirred in anhydrous DMF (3 mL) at room temperature overnight. Crude product was purified by column chromatography on silica gel (0−100% AcOEt in hexane) and yielded **2d** (192 mg, 52%) as a white solid. ^{1}H NMR (600 MHz, $CDCl_3$) δ: 9.87 (s, 1H), 7.53 (ddd, J = 10.8, 5.8, 5.0 Hz, 1H), 7.49−7.35 (m, 8H), 7.29 (dd, J = 7.5, 1.6 Hz, 1H), 7.01 (d, J = 8.2 Hz, 1H), 5.37 (s, 2H), 4.00 (s, 3H). ^{13}C NMR (151 MHz, $CDCl_3$) δ: 191.1, 153.4, 150.2, 143.6, 141.3, 136.2, 130.8, 130.7, 129.6, 128.2, 127.8, 127.6, 127.3, 126.8, 122.2, 112.6, 109.6, 71.0, 56.3. IR (ATR): 2916, 2850, 2834, 1683, 1588, 1507, 1421, 1265, 1235, 1134, 1031 cm^{-1}. HRMS ESI−MS-q-TOF for $C_{21}H_{17}BrO_3$ $[M + Na]^+$ found, 419.0253 m/z; calcd mass, 419.0259. Mp: 109.0 °C. UPLC−MS (DAD/ESI): t_R = 8.50 min, for $C_{21}H_{17}BrO_3$ $[M + H]^+$ found, 397.22 m/z; calcd mass, 397.04.

*Methyl 3-Bromo-4-((2-bromo-[1,1′-biphenyl]-3-yl)methoxy)-benzoate (**2e**).* Compound **2e** was prepared according to the protocol for **2a**. Preparation involved the use of **1a** (200 mg, 0.61 mmol), methyl 3-bromo-4-hydroxybenzoate (142 mg, 0.61 mmol), and potassium carbonate (169 mg, 1.22 mmol), which were stirred in anhydrous DMF (3 mL) at room temperature overnight. Crude product was purified by precipitation from AcOEt to give **2e** (131 mg, 45%) as a white solid. ^{1}H NMR (600 MHz, $CDCl_3$) δ: 8.30 (d, J = 2.1 Hz, 1H), 7.99 (dd, J = 8.6, 2.1 Hz, 1H), 7.71−7.68 (m, 1H), 7.47−7.38 (m, 6H), 7.30 (dd, J = 7.5, 1.7 Hz, 1H), 7.01 (d, J = 8.6 Hz, 1H), 5.32 (s, 2H), 3.90 (s, 3H). ^{13}C NMR (151 MHz, $CDCl_3$) δ: 165.7, 158.3, 143.4, 141.1, 135.9, 135.0, 130.6, 129.5, 128.0, 127.7, 127.5, 127.1, 124.3, 121.8, 112.5, 112.1, 70.8, 52.2. IR (ATR): 2948, 2163, 1981, 1781, 1599, 1498, 1431, 1363, 1311, 1269, 1240, 1108, 1054 cm^{-1}. HRMS ESI−MS-q-TOF for $C_{21}H_{16}Br_2O_3$ $[M + Na]^+$ found, 496.9447 m/z; calcd mass, 496.9364. Mp: 160.3 °C. UPLC−MS (DAD/ESI): t_R = 9.99 min, for $C_{21}H_{16}Br_2O_3$ $[M + H]^+$ found, 475.12 m/z; calcd mass, 474.95.

*4-(3-(3-Bromo-4-((2-bromo-[1,1′-biphenyl]-3-yl)methoxy)-benzamido)propyl)morpholin-4-ium Hydrochloride (**2f**).* **2e** (100 mg, 0.21 mmol) and DBU (350 μL) were stirred in 3-morpholinopropan-1-amine (1.5 mL) at room temperature for 2 days. Afterward, the reaction mixture was solubilized with AcOEt (30 mL). Following that, water was added (30 × 2 mL) to wash out the excess of amine from organic layers. Organic layers were dried, combined, and concentrated. Purification involved column chromatography on silica gel (0−10% $CHCl_3$ in MeOH). After purification, compound was converted into the corresponding hydrochloride salt, and product was precipitated from AcOEt to give **2f** (30 mg, 25%) as a white solid. ^{1}H NMR (600 MHz, $CDCl_3$) δ: 8.14 (t, J = 4.0 Hz, 1H), 8.06 (d, J = 2.2 Hz, 1H), 7.82 (dd, J = 8.6, 2.2 Hz, 1H), 7.73−7.69 (m, 1H), 7.48−7.37 (m, 5H), 7.30 (dd, J = 7.5, 1.7 Hz, 1H), 7.03 (d, J = 8.6 Hz, 1H), 5.31 (s, 2H), 3.78 (t, J = 4.6 Hz, 4H), 3.57 (dd, J = 10.9, 5.8 Hz, 2H), 2.58 (t, J = 5.7 Hz, 2H), 2.53 (s, 4H), 1.84−1.74 (m, 2H). ^{13}C NMR (151 MHz, $CDCl_3$) δ: 165.6, 157.1, 143.5, 141.2, 136.2, 132.1, 130.7, 129.6, 129.0, 128.2, 128.2, 127.8, 127.6, 127.2, 121.9, 113.0, 112.3, 70.9, 67.1, 59.2, 54.1, 41.1, 23.9. IR (ATR): 3460, 3299, 2951, 2856, 2822, 1626, 1604, 1553, 1497, 1285, 1267, 1118, 1056 cm^{-1}. HRMS ESI−MS-q-TOF for $[C_{27}H_{29}Br_2N_2O_3]^+$ [M] found, 587.0556 m/z; calcd mass, 587.0545. Mp: 128.9 °C. UPLC−MS (DAD/ESI): t_R = 6.75 min, for $[C_{27}H_{29}Br_2N_2O_3]^+$ [M] found, 587.12 m/z; calcd mass, 587.05.

*N-(2-((3-Bromo-4-((2-bromo-[1,1′-biphenyl]-3-yl)methoxy)-benzyl)amino)ethyl)acetamide (**2g**).* A solution of **2b** (200 mg, 0.45 mmol), *N*-(2-aminoethyl)acetamide (209 mg, 2.05 mmol), and AcOH (3 droplets) was stirred in anhydrous DMF (4 mL) at 25 °C for 2 h. $NaBH_3CN$ (132 mg, 2.24 mmol) then was added, and the resulted mixture was stirred additionally for 20 h. The residue was concentrated under reduced pressure. Water was added (30 mL), and the mixture was extracted with AcOEt (2 × 30 mL). Organic layers were combined, dried over $MgSO_4$, filtered, and concentrated. The crude product was purified by column chromatography (silica gel, 0−30% MeOH in $CHCl_3$) to give an off-white solid (126 mg, yield: 53%) as a product. ^{1}H NMR (600 MHz, DMSO) δ: 7.84 (s, 1H), 7.66 (dd, J = 7.6, 1.6 Hz, 1H), 7.62 (d, J = 1.9 Hz, 1H), 7.52 (t, J = 7.6 Hz, 1H), 7.49−7.45 (m, 2H), 7.44−7.30 (m, 5H), 7.17 (d, J = 8.5 Hz, 1H), 5.26 (s, 2H), 3.68 (s, 2H), 3.14 (q, J = 6.3 Hz, 2H), 2.55 (t, J = 6.5 Hz, 2H), 1.79 (s, 3H). ^{13}C NMR (151 MHz, DMSO) δ: 169.7, 153.6, 143.4, 141.2, 137.0, 133.2, 131.3, 129.7, 129.3, 128.8, 128.6, 128.2, 122.9, 114.2, 111.4, 71.0, 51.5, 48.2, 38.7, 23.1. IR (ATR): 3280, 3051, 2937, 2829, 2659, 1654, 1556, 1499, 1445, 1369, 1282, 1259, 1056 cm^{-1}. HRMS ESI−MS-q-TOF for $C_{24}H_{24}Br_2N_2O_2$ $[M + H]^+$ found, 531.0274 m/z; calcd mass, 531.0283. Mp: 142.9 °C. UPLC−MS (DAD/ESI): t_R = 6.13 min, for $C_{24}H_{24}Br_2N_2O_2$ $[M + H]^+$ found, 531.22 m/z; calcd mass, 531.03.

*(S)-1-(4-((2-Bromo-[1,1′-biphenyl]-3-yl)methoxy)benzyl)-piperidine-2-carboxylic Acid (**2h**).* Compound **2h** was prepared following the protocol of **2g**, using **2a** (90 mg, 0.25 mmol), L-pipecolinic acid (145 mg, 1.22 mmol), $NaBH_3CN$ (72 mg, 1.23 mmol), AcOH (3 droplets), and DMF (4 mL). The crude product was purified

https://dx.doi.org/10.1021/acs.jmedchem.0c01260
J. Med. Chem. 2020, 63, 11271−11285

by flash chromatography (silica gel, 0−50% MeOH in $CHCl_3$) to give a white solid (77 mg, yield: 65%) as the product. ^{1}H NMR (600 MHz, DMSO) δ: 7.59 (d, J = 7.1 Hz, 1H), 7.54−7.25 (m, 9H), 7.04 (d, J = 7.9 Hz, 2H), 5.19 (s, 2H), 4.01 (d, J = 11.9 Hz, 1H), 3.11 (s, 1H), 2.98 (s, 1H), 2.40 (s, 1H), 1.87 (s, 1H), 1.69 (s, 1H), 1.61−1.43 (m, 3H), 1.35 (s, 1H). ^{13}C NMR (151 MHz, DMSO) δ: 158.4, 143.5, 141.3, 137.2, 131.8, 131.4, 129.7, 129.5, 128.6, 128.2, 123.4, 115.0, 79.6, 70.3, 58.3, 49.6, 28.5, 23.9, 22.2. IR (ATR): 3055, 2940, 2862, 2352, 2251, 1610, 1513, 1447, 1413, 1386, 1242, 1180, 1028 cm^{-1}. HRMS ESI−MS-q-TOF for $C_{26}H_{26}BrNO_3$ $[M + H]^+$ found, 480.1169 m/z; calcd mass, 480.1174. Mp: 182.5 °C. UPLC−MS (DAD/ESI): t_R = 6.18 min, for $C_{26}H_{26}BrNO_3$ $[M + H]^+$ found, 480.24 m/z; calcd mass, 480.12.

*(S)-1-(4-((2-Bromo-[1,1′-biphenyl]-3-yl)methoxy)-3-methylbenzyl)piperidine-2-carboxylic Acid (**2i**).* Compound **2i** was obtained according to the procedure of **2g**, using **2c** (90 mg, 0.24 mmol), L-pipecolinic acid (140 mg, 1.08 mmol), $NaBH_3CN$ (69 mg, 1.18 mmol), AcOH (3 droplets), and DMF (4 mL). The crude product was purified by flash chromatography (silica gel, 0−50% MeOH in $CHCl_3$) to give a yellow solid (65 mg, yield: 56%) as a product. ^{1}H NMR (600 MHz, $CDCl_3$) δ: 7.50 (d, J = 7.5 Hz, 1H), 7.44−7.21 (m, 9H), 6.83 (d, J = 7.0 Hz, 1H), 5.06 (s, 2H), 4.39 (d, J = 55.8 Hz, 2H), 3.42 (d, J = 55.1 Hz, 2H), 2.62 (s, 1H), 2.28 (s, 3H), 1.96 (d, J = 9.0 Hz, 2H), 1.85−1.69 (m, 2H), 1.37−1.20 (m, 2H). ^{13}C NMR (151 MHz, $CDCl_3$) δ: 157.8, 143.5, 141.3, 137.0, 134.3, 130.9, 130.6, 129.6, 128.1, 127.9, 127.8, 127.3, 127.2, 122.4, 111.6, 70.1, 58.5, 50.9, 29.8, 28.2, 22.8, 22.1, 16.7. IR (ATR): 2943, 2862, 2390, 2250, 1613, 1505, 1447, 1410, 1288, 1258, 1137, 1003 cm^{-1}. HRMS ESI−MS-q-TOF for $C_{27}H_{28}BrNO_3$ $[M + H]^+$ found, 494.1325 m/z; calcd mass, 494.1330. Mp: 106.3 °C. UPLC−MS (DAD/ESI): t_R = 6.54 min, for $C_{27}H_{28}BrNO_3$ $[M + H]^+$ found, 494.26 m/z; calcd mass, 494.1330.

*(S)-1-(4-((2-Bromo-[1,1′-biphenyl]-3-yl)methoxy)-3-methoxybenzyl)piperidine-2-carboxylic Acid (**2j**).* Compound **2j** was obtained as described for **2g**. Preparation involved the use of **2d** (100 mg, 0.25 mmol), L-pipecolinic acid (149 mg, 1.15 mmol), $NaBH_3CN$ (74 mg, 1.26 mmol), AcOH (3 droplets), and DMF (4 mL). The crude product was purified by flash chromatography (silica gel, 0−50% MeOH in $CHCl_3$) to give a white solid (93 mg, yield: 72%) as a product. ^{1}H NMR (600 MHz, DMSO) δ: 7.60 (dd, J = 7.6, 1.5 Hz, 1H), 7.52−7.33 (m, 7H), 7.09 (s, 1H), 7.05 (d, J = 8.2 Hz, 1H), 6.94 (d, J = 7.9 Hz, 1H), 5.17 (s, 2H), 4.08 (d, J = 12.8 Hz, 1H), 3.80 (s, 3H), 3.15 (s, 1H), 3.04 (s, 1H), 1.96−1.87 (m, 1H), 1.72 (d, J = 9.7 Hz, 1H), 1.61−1.53 (m, 3H), 1.41−1.33 (m, 1H). ^{13}C NMR (151 MHz, DMSO) δ: 149.4, 147.9, 143.4, 141.3, 137.4, 131.4, 129.7, 129.3, 128.6, 128.2, 123.3, 123.1, 114.5, 113.7, 79.6, 71.0, 58.5, 56.1, 49.7, 28.3, 23.6, 22.1. IR (ATR): 3345, 3055, 2939, 2867, 2394, 2251, 1633, 1606, 1517, 1448, 1416, 1268, 1238, 1102, 1029 cm^{-1}. HRMS ESI−MS-q-TOF for $C_{27}H_{28}BrNO_4$ $[M + H]^+$ found, 510.1274 m/z; calcd mass, 510.1280. Mp: 154.6 °C. UPLC−MS (DAD/ESI): t_R = 6.10 min, for $C_{27}H_{28}BrNO_4$ $[M + H]^+$ found, 510.28 m/z; calcd mass, 510.13.

*(S)-1-(3-Bromo-4-((2-bromo-[1,1′-biphenyl]-3-yl)methoxy)-benzyl)piperidine-2-carboxylic Acid (**2k**).* Compound **2k** was prepared following the protocol of **2g**, using **2b** (119 mg, 0.27 mmol), L-pipecolinic acid (158 mg, 1.22 mmol), $NaBH_3CN$ (79 mg, 1.33 mmol), and AcOH (3 droplets), which were stirred in DMF (4 mL). The crude product was purified by flash chromatography (silica gel, 0−50% MeOH in $CHCl_3$) to give a white solid (77 mg, yield: 51%) as the product. ^{1}H NMR (600 MHz, DMSO) δ: 7.67 (d, J = 6.5 Hz, 1H), 7.62 (s, 1H), 7.52 (t, J = 7.6 Hz, 1H), 7.50−7.35 (m, 6H), 7.32 (d, J = 7.9 Hz, 1H), 7.18 (d, J = 8.4 Hz, 1H), 5.26 (s, 2H), 3.84 (d, J = 13.3 Hz, 1H), 3.49−3.39 (m, 1H), 3.05 (s, 1H), 2.90−2.83 (m, 1H), 2.24−2.16 (m, 1H), 1.86−1.76 (m, 1H), 1.74−1.62 (m, 1H), 1.58−1.40 (m, 3H), 1.39−1.29 (m, 1H). ^{13}C NMR (151 MHz, DMSO) δ: 153.4, 142.9, 140.7, 136.5, 133.7, 130.9, 129.8, 129.2, 128.3, 128.2, 127.7, 122.4, 113.6, 110.9, 70.6, 64.4, 57.8, 49.2, 28.7, 24.4, 22.0. IR (ATR): 3649, 3075, 2941, 2859, 2392, 2251, 1621, 1496, 1411, 1288, 1260, 1102, 1055 cm^{-1}. HRMS ESI−MS-q-TOF for $C_{26}H_{25}Br_2NO_3$ $[M + Na]^+$ found, 580.0097 m/z; calcd mass, 580.0099. Mp: 129.1 °C. UPLC−MS (DAD/ESI): t_R = 6.51 min, for $C_{26}H_{25}Br_2NO_3$ $[M + H]^+$ found, 558.20 m/z; calcd mass, 558.02.

*4-((2-Bromo-[1,1′-biphenyl]-3-yl)methoxy)-5-chloro-2-hydroxybenzaldehyde (**3a**).* 5-Chloro-2,4-dihydroxybenzaldehyde (657 mg, 2.43 mmol) and $NaHCO_3$ (200 mg, 2.43 mmoL) were dissolved in dry ACN (13 mL) and stirred for 20 min. To the resulted mixture was added dropwise **1a** (528 mg, 1.62 mmol) in dry DMF (18 mL). The solution was allowed to stir at room temperature for 20 h. The residue was concentrated under reduced pressure. Water was added (60 mL), and the mixture was extracted with AcOEt (2 × 60 mL). Organic layers were combined, dried over $MgSO_4$, filtered, and concentrated. The crude product was purified by flash chromatography (silica gel, 0−100% AcOEt in hexane) and yielded a white solid (368 mg, yield: 54%) as a product. ^{1}H NMR (600 MHz, $CDCl_3$) δ: 11.43 (s, 1H), 9.72 (s, 1H), 7.62 (dd, J = 7.7, 0.7 Hz, 1H), 7.58 (s, 1H), 7.47−7.38 (m, 6H), 7.32 (dd, J = 7.5, 1.4 Hz, 1H), 6.61 (s, 1H), 5.30 (d, J = 4.3 Hz, 2H). ^{13}C NMR (151 MHz, $CDCl_3$) δ: 193.9, 163.1, 160.7, 143.7, 141.1, 135.4, 134.2, 131.0, 129.6, 128.2, 127.9, 127.6, 127.1, 122.1, 115.4, 114.9, 102.0, 71.2 ppm. IR (ATR): 2925, 2850, 1644, 1618, 1490, 1360, 1274, 1200, 1056 cm^{-1}. HRMS ESI−MS-q-TOF for $C_{20}H_{14}BrClO_3$ $[M + Na]^+$ found, 438.9691 m/z; calcd mass, 438.9713. Mp: 192.8 °C. UPLC−MS (DAD/ESI): t_R = 9.34 min, for $C_{20}H_{14}BrClO_3$ $[M + H]^+$ found, 417.09 m/z; calcd mass, 416.99.

*4-((5-((2-Bromo-[1,1′-biphenyl]-3-yl)methoxy)-4-chloro-2-formylphenoxy)methyl)picolinonitrile (**3b**).* **3a** (224 mg, 0.54 mmol), 4-(bromomethyl)picolinonitrile (235 mg, 1.19 mmol), and potassium carbonate (507 mg, 3.67 mmol) were stirred in anhydrous DMF (18 mL) at room temperature overnight. The solvent was removed under reduced pressure. Water was added (30 mL), and the mixture was extracted with AcOEt (2 × 30 mL). Organic layers were combined and concentrated. Purification involved flash chromatography (0−100% AcOEt in hexane) and yielded **3b** (180 mg, 63%) as a white solid. ^{1}H NMR (600 MHz, $CDCl_3$) δ: 10.34 (s, 1H), 8.74 (d, J = 5.1 Hz, 1H), 7.95 (s, 1H), 7.72 (d, J = 0.7 Hz, 1H), 7.61−7.55 (m, 2H), 7.51−7.29 (m, 7H), 6.51 (s, 1H), 5.35 (s, 2H), 5.21 (s, 2H). ^{13}C NMR (151 MHz, $CDCl_3$) δ: 186.4, 159.9, 159.6, 151.7, 146.5, 143.8, 141.0, 135.3, 134.7, 131.3, 131.2, 129.5, 128.3, 128.1, 128.0, 127.4, 125.9, 124.3, 122.1, 119.7, 117.5, 117.0, 98.7, 71.1, 68.4. IR (ATR): 2923, 28853, 2237, 1677, 1598, 1500, 1444, 1380, 123, 1280, 1213, 1038 cm^{-1}. HRMS ESI−MS-q-TOF for $C_{27}H_{18}BrClN_2O_3$ $[M + Na]^+$ found, 555.0107 m/z; calcd mass, 555.0087. Mp: 199.7 °C. UPLC−MS (DAD/ESI): t_R = 9.20 min, for $C_{27}H_{18}BrClN_2O_3$ $[M + H]^+$ found, 533.21 m/z; calcd mass, 533.03.

*3-((5-((2-Bromo-[1,1′-biphenyl]-3-yl)methoxy)-4-chloro-2-formylphenoxy)methyl)benzonitrile (**3c**).* Compound **3c** was prepared following the protocol of **3b**, using **3a** (135 mg, 0.33 mmol), 3-(bromomethyl)benzonitrile (76 mg, 0.39 mmol), and potassium carbonate (89 mg, 0.65 mmol), which were stirred in anhydrous DMF (4 mL). Purification involved crystallization from AcOEt and gave **2e** (150 mg, 87%) as a white solid. ^{1}H NMR (600 MHz, $CDCl_3$) δ: 10.32 (s, 1H), 7.93 (s, 1H), 7.70 (s, 1H), 7.67−7.60 (m, 3H), 7.52 (t, J = 7.7 Hz, 1H), 7.48−7.40 (m, 4H), 7.40−7.36 (m, 2H), 7.33 (dd, J = 7.5, 1.6 Hz, 1H), 6.57 (s, 1H), 5.32 (s, 2H), 5.18 (s, 2H). ^{13}C NMR (151 MHz, $CDCl_3$) δ: 186.8, 160.7, 159.5, 143.7, 141.0, 137.2, 135.5, 132.3, 131.6, 131.2, 130.7, 130.5, 129.9, 129.5, 128.3, 128.0, 127.9, 127.4, 122.1, 119.7, 118.4, 117.0, 113.3, 98.9, 71.0, 70.0. IR (ATR): 2919, 2856, 2225, 1678, 1595, 1441, 1408, 1380, 1320, 1277, 1199, 1066 cm^{-1}. HRMS ESI−MS-q-TOF for $C_{28}H_{19}BrClNO_3$ $[M + Na]^+$ found, 554.0112 m/z; calcd mass, 554.0135. Mp: 189.4 °C. UPLC−MS (DAD/ESI): t_R = 9.64 min, for $C_{28}H_{19}BrClNO_3$ $[M + H]^+$ found, 532.15 m/z; calcd mass, 532.03.

*4-([1,1′:2′,1″-Terphenyl]-3′-ylmethoxy)-5-chloro-2-hydroxybenzaldehyde (**3e**).* 5-Chloro-2,4-dihydroxybenzaldehyde (657 mg, 3.81 mmol), PPh_3 (11.07 g, 42.21 mmol), and **1b** (1000 mg, 3.84 mmol) were dissolved in dry THF (30 mL). To the ice-cooled solution of the resulted mixture was added dropwise DIAD (0.83 mL, 4.23 mmol) in THF (30 mL). The solution was allowed to warm to room temperature and was stirred for 20 h. The mixture was concentrated under reduced pressure. The crude product was purified by column chromatography on silica gel using 0−60% AcOEt in hexane to give a white solid (313 mg, yield: 20%). ^{1}H NMR (600 MHz, $CDCl_3$) δ: 11.36 (s, 1H), 9.66 (s, 1H), 7.67 (d, J = 6.7 Hz, 1H), 7.54−7.48 (m, 2H), 7.45 (dd, J = 7.7, 1.2

https://dx.doi.org/10.1021/acs.jmedchem.0c01260
J. Med. Chem. 2020, 63, 11271−11285

Hz, 1H), 7.24−7.06 (m, 10H), 6.26 (s, 1H), 4.93 (s, 2H). ^{13}C NMR (151 MHz, $CDCl_3$) δ: 193.7, 162.8, 160.8, 142.0, 141.1, 139.9, 138.2, 133.9, 133.4, 130.3, 130.2, 129.8, 128.0, 127.9, 127.6, 127.2, 127.1, 126.4, 114.9, 114.7, 101.5, 69.7. IR (ATR): 3055, 2920, 2851, 1638, 1622, 1573, 1482, 1326, 1269, 1199, 1181, 1047 cm^{-1}. HRMS ESI−MS-q-TOF for $C_{26}H_{19}ClO_3$ $[M + Na]^+$ found, 437.0915 m/z; calcd mass, 437.0920. Mp: 152.4 °C. UPLC−MS (DAD/ESI): t_R = 9.51 min, for $C_{26}H_{19}ClO_3$ $[M + H]^+$ found, 415.30 m/z; calcd mass, 415.11.

*4-((5-([1,1′:2′,1″-Terphenyl]-3′-ylmethoxy)-4-chloro-2-formylphenoxy)methyl)picolinonitrile (**3f**).* Compound **3f** was prepared following the protocol of **3b**, using **3e** (278 mg, 0.67 mmol), 4-(bromomethyl)picolinonitrile (159 mg, 0.81 mmol), K_2CO_3 (185 mg, 1.34 mmol), and anhydrous DMF (4 mL). The product was isolated by crystallization from AcOEt as a white solid (175 mg, yield: 90%). ^{1}H NMR (600 MHz, $CDCl_3$) δ: 10.27 (s, 1H), 8.73 (d, J = 5.0 Hz, 1H), 7.88 (s, 1H), 7.66 (d, J = 0.6 Hz, 1H), 7.63 (dd, J = 7.5, 1.3 Hz, 1H), 7.52−7.44 (m, 3H), 7.23−7.19 (m, 3H), 7.18−7.12 (m, 3H), 7.10−7.02 (m, 4H), 6.14 (s, 1H), 5.04 (s, 2H), 4.95 (s, 2H). ^{13}C NMR (151 MHz, $CDCl_3$) δ: 186.3, 159.7, 159.6, 151.5, 146.4, 142.1, 140.9, 139.8, 138.3, 134.5, 133.2, 130.9, 130.6, 130.3, 129.8, 128.1, 128.0, 127.7, 127.4, 127.2, 126.6, 125.8, 124.2, 119.2, 117.3, 116.9, 98.3, 69.8, 68.1. IR (ATR): 3060, 2875, 2242, 1673, 1595, 1499, 1449, 1402, 1320, 1278, 1263, 1166, 1034 cm^{-1}. HRMS ESI−MS-q-TOF for $C_{33}H_{23}ClN_2O_3$ $[M + Na]^+$ found, 553.1289 m/z; calcd mass, 553.1295. Mp: 196.7 °C. UPLC−MS (DAD/ESI): t_R = 9.32 min, for $C_{33}H_{23}ClN_2O_3$ $[M + H]^+$ found, 531.35 m/z; calcd mass, 531.15.

*3-Bromo-4-((2-bromo-3-(2,3-dihydrobenzo[b][1,4]dioxin-6-yl)-benzyl)oxy)benzaldehyde (**4a**).* Compound **4a** was prepared as described in the protocol of **2a**, using **1g** (250 mg, 0.65 mmol), 3-bromo-4-hydroxybenzaldehyde (130 mg, 0.65 mmol), potassium carbonate (180 mg, 1.31 mmol), and anhydrous DMF (4 mL). Crude product was purified by column chromatography on silica gel (0−100% AcOEt in hexane) and yielded **4a** (291 mg, 88%) as a white solid. ^{1}H NMR (600 MHz, DMSO) δ: 9.88 (s, 1H), 8.15 (d, J = 2.0 Hz, 1H), 7.97 (dd, J = 8.5, 2.0 Hz, 1H), 7.64 (dd, J = 7.6, 1.6 Hz, 1H), 7.52−7.44 (m, 2H), 7.35 (dd, J = 7.6, 1.7 Hz, 1H), 6.94 (d, J = 8.3 Hz, 1H), 6.87 (d, J = 2.1 Hz, 1H), 6.84 (dd, J = 8.2, 2.1 Hz, 1H), 5.40 (s, 2H), 4.29 (s, J = 4.6 Hz, 4H). ^{13}C NMR (151 MHz, DMSO) δ: 190.7, 159.0, 143.2, 142.9, 142.5, 135.8, 134.1, 133.8, 131.3, 131.2, 131.0, 128.5, 127.8, 122.9, 122.3, 118.0, 116.8, 114.1, 111.9, 71.2, 64.2. IR (ATR): 2983, 2952, 1685, 1598, 1494, 1314, 1275, 1258, 1243, 1190, 1062 cm^{-1}. HRMS ESI−MS-q-TOF for $C_{22}H_{16}Br_2O_4$ $[M + Na]^+$ found, 524.9348 m/z; calcd mass, 524.9313. Mp: 196.2 °C. UPLC−MS (DAD/ESI): t_R = 8.98 min, for $C_{22}H_{16}Br_2O_4$ $[M + H]^+$ found, 503.04 m/z; calcd mass, 502.95.

*(S)-1-(3-Bromo-4-((2-bromo-3-(2,3-dihydrobenzo[b][1,4]dioxin-6-yl)benzyl)oxy)benzyl)piperidine-2-carboxylic Acid (**4b**).* Compound **4b** was prepared according to the procedure of **2g**, using **4a** (310 mg, 0.61 mmol), L-pipecolinic acid (364 mg, 2.82 mmol), $NaBH_3CN$ (181 mg, 3.07 mmol), addition of AcOH (3 droplets), and anhydrous DMF (4 mL) as a solvent. The crude product was purified by flash chromatography (silica gel, 0−50% MeOH in $CHCl_3$) to give a white solid (164 mg, yield: 43%) as the product. ^{1}H NMR (600 MHz, DMSO) δ: 7.66−7.59 (m, 2H), 7.48 (t, J = 7.6 Hz, 1H), 7.35−7.29 (m, 2H), 7.18 (d, J = 8.5 Hz, 1H), 6.93 (d, J = 8.2 Hz, 1H), 6.86 (d, J = 2.1 Hz, 1H), 6.83 (dd, J = 8.3, 2.1 Hz, 1H), 5.24 (s, 2H), 4.28 (s, 4H), 3.85 (d, J = 13.4 Hz, 1H), 3.06 (dd, J = 8.2, 3.8 Hz, 1H), 2.93−2.81 (m, 1H), 2.30−2.17 (m, J = 16.9, 8.1 Hz, 1H), 1.86−1.77 (m, 1H), 1.74−1.61 (m, J = 12.6, 6.6 Hz, 1H), 1.57−1.41 (m, 3H), 1.38−1.28 (m, 1H), 1.23 (s, 1H). ^{13}C NMR (151 MHz, DMSO) δ: 153.6, 143.1, 142.8, 142.4, 136.5, 133.8, 133.7, 131.0, 129.9, 128.2, 127.7, 122.7, 122.3, 118.0,116.8, 113.7, 111.0, 70.7, 64.2, 57.9, 49.2, 28.6, 28.5, 24.1, 22.0. IR (ATR): 2932, 2864, 2356, 2323, 2286, 1728, 1634, 1589, 1500, 1454, 1368, 1315, 1278, 1260, 1246, 1197, 1065 cm^{-1}. HRMS ESI−MS-q-TOF for $C_{28}H_{27}Br_2NO_5$ $[M + H]^+$ found, 616.0327 m/z; calcd mass, 616.0334. Mp: decomposition at 191.9 °C. UPLC−MS (DAD/ESI): t_R = 6.25 min, for $C_{28}H_{27}Br_2NO_5$ $[M + H]^+$ found, 616.23 m/z; calcd mass, 616.03.

*3-Bromo-4-((3-(2,3-dihydrobenzo[b][1,4]dioxin-6-yl)-2-fluorobenzyl)oxy)benzaldehyde (**4c**).* **1d** (700 mg, 2.69 mmoL) was dissolved in anhydrous DCM (10 mL) under Ar. $SOCl_2$ (3.2 mL) was added carefully, and the resulted mixture was stirred at 45 °C. After 3 h the reaction was stopped, and the mixture was concentrated under reduced pressure. Generated in situ chloride, 3-bromo-4-hydroxybenzaldehyde (1.6 g, 8.08 mmol), and K_2CO_3 (1.8 g, 13.46 mmol) were stirred in anhydrous DMF (10 mL) at room temperature overnight. The solvent was removed under reduced pressure. Water was added (100 mL), and the mixture was extracted with AcOEt (2 × 100 mL). Organic layers were combined and concentrated. The crude product was chromatographed on silica gel eluting with 0−60% AcOEt in hexane to give 180 mg of a white solid with a yield of 30%. ^{1}H NMR (600 MHz, $CDCl_3$) δ: 9.85 (s, 1H), 8.12 (d, J = 2.0 Hz, 1H), 7.81 (dd, J = 8.5, 2.0 Hz, 1H), 7.55 (t, J = 7.1 Hz, 1H), 7.39 (td, J = 7.6, 1.6 Hz, 1H), 7.23 (t, J = 7.7 Hz, 1H), 7.12 (d, J = 8.5 Hz, 1H), 7.09 (t, J = 1.7 Hz, 1H), 7.04 (dt, J = 8.3, 1.8 Hz, 1H), 6.95 (d, J = 8.4 Hz, 1H), 5.36 (s, 2H), 4.31 (s, 4H). ^{13}C NMR (151 MHz, $CDCl_3$) δ: 189.7, 159.7, 157.0 (d, $^1J_{C-F}$ = 248.2 Hz), 143.6 (d, $^2J_{C-F}$ = 14.0 Hz), 134.8, 131.3, 131.2, 130.7 (d, $^3J_{C-F}$ = 3.1 Hz), 128.8, 128.7, 128.7, 127.8 (d, $^3J_{C-F}$ = 3.1 Hz), 124.7 (d, $^3J_{C-F}$ = 3.8 Hz), 123.6 (d, $^2J_{C-F}$ = 15.1 Hz), 122.4, 118.1, 117.5, 113.4, 113.0, 65.2 (d, $^3J_{C-F}$ = 6.3 Hz), 64.6, 64.5. IR (ATR): 2927, 2823, 2738, 1691, 1592, 1493, 1450, 1323, 1278, 1191, 1064, 1047 cm^{-1}. HRMS ESI−MS-q-TOF for $C_{22}H_{16}BrFO_4$ $[M + Na]^+$ found, 465.0109 m/z; calcd mass, 465.0114. Mp: 118.0 °C. UPLC−MS (DAD/ESI): t_R = 8.56 min, for $C_{22}H_{16}BrFO_4$ $[M + H]^+$ found, 443.15 m/z; calcd mass, 443.03.

*N-(2-((3-Bromo-4-((3-(2,3-dihydrobenzo[b][1,4]dioxin-6-yl)-2-fluorobenzyl)oxy)benzyl)amino)ethyl)acetamide (**4d**).* Compound **4d** was prepared following the procedure of **2g**, using **4c** (120 mg, 0.27 mmol), *N*-(2-aminoethyl)acetamide (126 mg, 1.24 mmol), $NaBH_3CN$ (79 mg, 1.35 mmol), addition of AcOH (3 droplets), and anhydrous DMF (4 mL) as a solvent. The crude product was purified by column chromatography (silica gel, 0−30% MeOH in $CHCl_3$) to give a white solid (88 mg, yield: 61%) as the product. ^{1}H NMR (600 MHz, $CDCl_3$) δ: 7.60 (d, J = 2.0 Hz, 1H), 7.55 (t, J = 6.4 Hz, 1H), 7.36 (td, J = 7.6, 1.6 Hz, 1H), 7.25 (d, J = 2.0 Hz, 1H), 7.21 (t, J = 7.6 Hz, 1H), 7.08 (t, J = 1.5 Hz, 1H), 7.04 (dt, J = 8.4, 1.8 Hz, 1H), 6.97 (d, J = 8.4 Hz, 1H), 6.94 (d, J = 8.4 Hz, 1H), 6.30 (s, 1H), 5.25 (s, 2H), 4.30 (s, 4H), 3.79 (s, 2H), 3.39 (dd, J = 11.1, 5.5 Hz, 2H), 2.84 (t, J = 5.6 Hz, 2H), 2.00 (s, 3H). ^{13}C NMR (151 MHz, $CDCl_3$) δ: 171.0, 157.0 (d, $^1J_{C-F}$ = 248.1 Hz), 154.6, 143.6 (d, $^3J_{C-F}$ = 6.9 Hz), 133.8, 131.5, 130.4 (d, $^4J_{C-F}$ = 2.6 Hz), 129.1, 128.8, 128.6 (d, $^2J_{C-F}$ = 13.3 Hz), 127.9 (d, $^3J_{C-F}$ = 3.2 Hz), 124.5 (d, $^3J_{C-F}$ = 3.7 Hz), 124.4 (d, $^2J_{C-F}$ = 15.2 Hz), 122.4, 118.1, 117.4, 113.9, 112.8, 65.0 (d, $^3J_{C-F}$ = 6.0 Hz), 64.6, 64.5, 52.1, 47.9, 38.7, 23.4. IR (ATR): 3283, 2925, 2803, 2163, 1692, 1655, 1578, 1502, 1454, 1417, 1373, 1319, 1283, 1261, 1244, 1192, 1128, 1066, 1048 cm^{-1}. HRMS ESI−MS-q-TOF for $C_{26}H_{26}BrFN_2O_4$ $[M + H]^+$ found, 529.1135 m/z; calcd mass, 529.1138. Mp: 121.6 °C. UPLC−MS (DAD/ESI): t_R = 5.66 min, $C_{26}H_{26}BrFN_2O_4$ $[M + H]^+$ found, 529.22 m/z; calcd mass, 529.11.

*4-([1,1′:2′,1″-Terphenyl]-3′-ylmethoxy)-3-bromobenzaldehyde (**4e**).* Compound **4e** was prepared following the procedure of **4c**. Preparation of chloride involved the use of **1b** (300 mg, 1.15 mmoL), which was dissolved in anhydrous DCM (4.5 mL) with the addition of $SOCl_2$ (1.4 mL) under Ar. In the second step, generated in situ chloride was stirred with 3-bromo-4-hydroxybenzaldehyde (231 mg, 1.15 mmol) and K_2CO_3 (319 mg, 2.31 mmol) in anhydrous DMF (3.3 mL) at room temperature overnight. The crude product was chromatographed on silica gel, eluting with 0−60% AcOEt in hexane to give 308 mg of an off-white solid with yield: 60%. ^{1}H NMR (600 MHz, $CDCl_3$) δ: 9.8 (s, 1H), 8.1 (d, J = 2.0 Hz, 1H), 7.7 (m, 1H), 7.7 (dd, J = 8.5, 2.0 Hz, 1H), 7.5 (t, J = 7.7 Hz, 1H), 7.4 (dd, J = 7.7, 1.2 Hz, 1H), 7.2−7.0 (m, 10H), 6.7 (d, J = 8.5 Hz, 1H), 5.0 (s, 2H). ^{13}C NMR (151 MHz, $CDCl_3$) δ: 189.7, 159.8, 142.0, 141.3, 139.8, 138.4, 134.7, 133.9, 131.1, 130.9, 130.4, 130.3, 129.9, 128.1, 128.0, 127.7, 127.3, 127.2, 126.5, 113.2, 112.9, 69.7. IR (ATR): 3029, 2733, 1685, 1592, 1285, 1263, 1194, 1005 cm^{-1}. HRMS ESI−MS-q-TOF for $C_{26}H_{19}BrO_2$ $[M + Na]^+$ found, 465.0465 m/z; calcd mass, 465.0466. Mp: 142.3 °C. UPLC−MS (DAD/ESI): t_R = 9.51 min, for $C_{26}H_{19}BrO_2$ $[M + H]^+$ found, 445.34 m/z; calcd mass, 445.06.

https://dx.doi.org/10.1021/acs.jmedchem.0c01260
J. Med. Chem. 2020, 63, 11271−11285

*(2S,4S)-1-(4-([1,1′:2′,1″-Terphenyl]-3′-ylmethoxy)-3-bromobenzyl)-4-hydroxypyrrolidine-2-carboxylic Acid (**4f**).* The synthesis of compound **4f** was performed following the procedure of **2g**. Preparation included the use of **4e** (200 mg, 0.45 mmol), (2*R*,4*R*)-4-hydroxypyrrolidine-2-carboxylic acid (272 mg, 2.07 mmol), $NaBH_3CN$ (142 mg, 2.26 mmol), AcOH (3 droplets), and anhydrous DMF (6.0 mL). The crude product was purified by flash chromatography (silica gel, 0−50% MeOH in AcOEt) to give a white solid (93 mg, yield: 37%) as the product. ^{1}H NMR (600 MHz, $CDCl_3$) δ: 7.7 (d, J = 7.2 Hz, 1H), 7.6−7.5 (m, 2H), 7.4 (dd, J = 7.7, 1.1 Hz, 1H), 7.2−7.1 (m, 9H), 7.1−7.0 (m, 2H), 6.7 (d, J = 8.4 Hz, 1H), 4.8 (s, 2H), 4.1 (s, 1H), 3.9 (d, J = 13.1 Hz, 1H), 3.5 (d, J = 13.0 Hz, 1H), 3.1 (s, J = 19.4 Hz, 1H), 2.8 (d, J = 9.4 Hz, 1H), 2.4 (s, 1H), 2.2 (s, 1H), 1.7 (d, J = 8.8 Hz, 1H), 1.2 (s, 1H). ^{13}C NMR (151 MHz, $CDCl_3$) δ: 153.4, 141.3, 141.0, 139.8, 138.0, 134.6, 133.6, 130.1, 129.9, 129.7, 129.5, 129.0, 127.8, 127.7, 127.7, 127.7, 126.9, 126.4, 113.2, 110.7, 68.8, 68.6, 65.4, 60.7, 55.8, 48.6. IR (ATR): 3297, 3057, 2659, 1600, 1494, 1410, 1253, 1050 cm^{-1}. HRMS ESI−MS-q-TOF for $C_{31}H_{28}BrNO_4$ $[M + Na]^+$ found, 580.1078 m/z; calcd mass, 580.1099. Mp: 152.3 °C. UPLC−MS (DAD/ESI): t_R = 6.55 min, for $C_{31}H_{28}BrNO_4$ $[M + H]^+$ found, 558.27 m/z; calcd mass, 558.13.

*2′-Bromo-3′-((2-bromo-4-formylphenoxy)methyl)-[1,1′-biphenyl]-4-carbonitrile (**4g**).* The synthesis of compound **4g** was performed according to the procedure of **2a**, using **1e** (559 mg, 1.59 mmol), 3-bromo-4-hydroxybenzaldehyde (320 mg, 1.59 mmol), potassium carbonate (440 mg, 3.18 mmol), and anhydrous DMF (8 mL). The product was precipitated from AcOEt and yielded **4g** (461 mg, 61%) as a white solid. ^{1}H NMR (600 MHz, $CDCl_3$) δ: 9.88 (s, 1H), 8.15 (d, J = 2.0 Hz, 1H), 7.84 (dd, J = 8.4, 2.0 Hz, 1H), 7.79−7.73 (m, 3H), 7.53−7.50 (m, 2H), 7.48 (t, J = 7.7 Hz, 1H), 7.28 (dd, J = 7.6, 1.6 Hz, 1H), 7.11 (d, J = 8.5 Hz, 1H), 5.34 (s, 2H). ^{13}C NMR (151 MHz, $CDCl_3$) δ: 189.6, 159.4, 145.6, 141.7, 136.3, 134.9, 132.1, 131.4, 131.3, 130.5, 128.3, 128.0, 121.3, 118.8, 113.4, 113.1, 111.9, 70.9. IR (ATR): 2844, 2227, 1688, 1590, 1566, 1489, 1276, 1256, 1184, 1050 cm^{-1}. HRMS ESI−MS-q-TOF for $C_{21}H_{13}Br_2NO_2$ $[M + Na]^+$ found, 491.9203 m/z; calcd mass, 491.9211. Mp: over 200 °C. UPLC−MS (DAD/ESI): t_R = 8.71 min, for $C_{21}H_{13}Br_2NO_2$ $[M + H]^+$ found, 469.93 m/z; calcd mass, 469.94.

*N-(2-((3-Bromo-4-((2-bromo-4′-cyano-[1,1′-biphenyl]-3-yl)methoxy)benzyl)amino)ethyl)acetamide (**4h**).* Compound **4h** was prepared following the procedure of **2g**, using **4g** (100 mg, 0.21 mmol), *N*-(2-aminoethyl)acetamide (99 mg, 0.97 mmol), $NaBH_3CN$ (63 mg, 1.06 mmol), addition of AcOH (3 droplets), and anhydrous DMF (5 mL) as a solvent. The crude product was purified by column chromatography (silica gel, 0−30% MeOH in $CHCl_3$) to give an off-white solid (30 mg, yield: 26%) as a product. ^{1}H NMR (600 MHz, $CDCl_3$) δ: 7.79 (d, J = 7.7 Hz, 1H), 7.74 (d, J = 8.3 Hz, 2H), 7.58 (d, J = 1.9 Hz, 1H), 7.51 (d, J = 8.3 Hz, 2H), 7.46 (t, J = 7.7 Hz, 1H), 7.25 (dd, J = 7.6, 1.5 Hz, 1H), 7.21 (dd, J = 8.3, 1.9 Hz, 1H), 6.94 (d, J = 8.4 Hz, 1H), 6.00 (s, 1H), 5.23 (s, 2H), 3.73 (s, 2H), 3.35 (dd, J = 11.3, 5.6 Hz, 2H), 2.76 (t, J = 5.8 Hz, 2H), 1.99 (s, 3H). ^{13}C NMR (151 MHz, $CDCl_3$) δ: 170.5, 153.9, 145.8, 141.5, 137.3, 134.5, 133.3, 132.1, 130.5, 130.1, 128.4, 128.4, 127.9, 121.2, 118.9, 113.7, 112.5, 111.8, 70.8, 52.5, 48.1, 39.2, 23.5. IR (ATR): 3282, 2925, 2228, 1688, 1654, 1591, 1554, 1490, 1447, 1362, 1279, 1256, 1185, 1052, 1025 cm^{-1}. HRMS ESI−MS-q-TOF for $C_{25}H_{23}Br_2N_3O_2$ $[M + H]^+$ found, 556.0230 m/z; calcd mass, 556.0235. Mp: 152.8 °C. UPLC−MS (DAD/ESI): t_R = 5.67 min, for $C_{25}H_{23}Br_2N_3O_2$ $[M + H]^+$ found, 556.21 m/z; calcd mass, 556.02.

*3-Bromo-4-((2-bromo-3′-fluoro-[1,1′-biphenyl]-3-yl)methoxy)benzaldehyde (**4i**).* Compound **4i** was obtained according to the procedure of **2a**, using **1f** (700 mg, 2.03 mmol), 4-hydroxy-3-methylbenzaldehyde (409 mg, 2.03 mmol), potassium carbonate (562 mg, 4.07 mmol), and anhydrous DMF (10 mL). Product was purified by precipitation from AcOEt and yielded **4i** (534 mg, 57%) as a white solid. ^{1}H NMR (600 MHz, $CDCl_3$) δ: 9.87 (s, 1H), 8.15 (d, J = 2.0 Hz, 1H), 7.83 (dd, J = 8.4, 2.0 Hz, 1H), 7.75−7.69 (m, 1H), 7.44 (t, J = 7.6 Hz, 1H), 7.42−7.38 (m, 1H), 7.30 (dd, J = 7.5, 1.7 Hz, 1H), 7.19−7.14 (m, 1H), 7.14−7.05 (m, 3H), 5.35 (s, 2H). ^{13}C NMR (151 MHz, $CDCl_3$) δ: 189.6, 162.5 (d, $^1J_{C-F}$ = 246.4 Hz), 159.5, 143.1 (d, $^3J_{C-F}$ = 7.9 Hz), 142.3, 135.9, 134.8, 131.3, 130.7, 129.8 (d, $^3J_{C-F}$ = 8.3 Hz), 127.8, 127.6, 125.4 (d, $^4J_{C-F}$ = 2.2 Hz), 121.7, 116.8 (d, $^2J_{C-F}$ = 22.0 Hz), 114.8 (d, $^2J_{C-F}$ = 21.0 Hz), 113.4, 113.1, 71.0. IR (ATR): 3060, 2922, 2853, 1683, 1594, 1490, 1461, 1418, 1368, 1313, 1278, 1255, 1190, 1049 cm^{-1}. HRMS ESI−MS-q-TOF for $C_{20}H_{13}Br_2FO_2$ $[M + Na]^+$ found, 484.9150 m/z; calcd mass, 484.9164. Mp: 168.1 °C. UPLC−MS (DAD/ESI): t_R = 9.32 min, for $C_{20}H_{13}Br_2FO_2$ $[M + H]^+$ found, 463.02 m/z; calcd mass, 462.93.

*(S)-1-(3-Bromo-4-((2-bromo-3′-fluoro-[1,1′-biphenyl]-3-yl)methoxy)benzyl)piperidine-2-carboxylic Acid (**4j**).* Compound **4j** was prepared following the procedure of **2g**, using **4i** (135 mg, 0.29 mmol), L-pipecolinic acid (172 mg, 1.33 mmol), $NaBH_3CN$ (86 mg, 1.45 mmol), addition of AcOH (3 droplets), and anhydrous DMF (5 mL) as a solvent. The crude product was purified by column chromatography (silica gel, 0−40% MeOH in $CHCl_3$) to give a white solid (73 mg, yield: 44%) as the product. ^{1}H NMR (600 MHz, DMF) δ: 7.82 (dd, J = 7.7, 1.5 Hz, 1H), 7.73 (s, 1H), 7.63−7.56 (m, 2H), 7.46−7.41 (m, 2H), 7.33−7.27 (m, 4H), 5.36 (s, 2H), 3.97 (d, J = 13.3 Hz, 1H), 3.56 (d, J = 12.8 Hz, 1H), 3.29−3.23 (m, 1H), 3.03−2.97 (m, 1H), 2.39−2.30 (m, 1H), 1.95−1.89 (m, 1H), 1.85−1.77 (m, 1H), 1.62−1.48 (m, 3H), 1.48−1.39 (m, 1H). ^{13}C NMR (151 MHz, DMF) δ: 175.0, 167.2 (d, $^1J_{C-F}$ = 63.5 Hz), 155.0, 144.4 (d, $^3J_{C-F}$ = 7.9 Hz), 143.1, 138.1, 134.9, 131.9, 131.2 (d, $^3J_{C-F}$ = 8.4 Hz), 130.9, 129.8, 128.9, 126.7, 123.2, 117.4 (d, $^2J_{C-F}$ = 22.2 Hz), 115.6 (d, $^2J_{C-F}$ = 21.0 Hz), 114.7, 112.3, 71.9, 65.4, 59.4, 50.5, 25.7, 24.0, 23.2. IR (ATR): 2923, 2853, 1614, 1495, 1461, 1363, 1288, 1259, 1196, 1157, 1055, 1023 cm^{-1}. HRMS ESI−MS-q-TOF for $C_{26}H_{24}Br_2FNO_3$ $[M + H]^+$ found, 576.0180 m/z; calcd mass, 576.0185. Mp: 175.6 °C. UPLC−MS (DAD/ESI): t_R = 6.65 min, for $C_{26}H_{24}Br_2FNO_3$ $[M + H]^+$ found, 576.15 m/z; calcd mass, 576.02.

*N-(2-((3-Bromo-4-((2-bromo-3′-fluoro-[1,1′-biphenyl]-3-yl)methoxy)benzyl)amino)ethyl)acetamide (**4k**).* Compound **4k** was prepared according to the procedure of **2g**, using **4i** (200 mg, 0.43 mmol), *N*-(2-aminoethyl)acetamide (201 mg, 1.97 mmol), $NaBH_3CN$ (127 mg, 2.16 mmol), addition of AcOH (3 droplets), and anhydrous DMF (4 mL) as a solvent. The crude product was purified by column chromatography (silica gel, 0−40% MeOH in $CHCl_3$) to give a white solid (159 mg, yield: 67%) as the product. ^{1}H NMR (600 MHz, DMSO) δ: 7.98 (t, J = 5.2 Hz, 1H), 7.70 (d, J = 1.9 Hz, 1H), 7.68 (dd, J = 7.7, 1.6 Hz, 1H), 7.56−7.49 (m, 2H), 7.41−7.37 (m, 2H), 7.30−7.19 (m, 4H), 5.27 (s, 2H), 3.81 (s, 2H), 3.21 (dd, J = 12.2, 6.2 Hz, 2H), 2.67 (t, J = 6.4 Hz, 2H), 1.80 (s, 3H). ^{13}C NMR (151 MHz, DMSO) δ: 169.6, 161.7 (d, $^1J_{C-F}$ = 244.0 Hz), 153.6, 142.9 (d, $^3J_{C-F}$ = 8.0 Hz), 141.7, 136.6, 133.4, 130.9, 130.3 (d, $^3J_{C-F}$ = 8.5 Hz), 129.6, 128.8, 127.9, 125.6, 122.3, 116.3 (d, $^2J_{C-F}$ = 22.0 Hz), 114.7 (d, $^2J_{C-F}$ = 20.8 Hz), 113.8, 111.0, 70.6, 50.4, 47.2, 37.3, 22.7. IR (ATR): 3282, 2934, 2774, 2427, 1656, 1557, 1500, 1446, 1363, 1291, 1261, 1195, 1070, 1056 cm^{-1}. HRMS ESI−MS-q-TOF for $C_{24}H_{23}Br_2FN_2O_2$ $[M + H]^+$ found, 549.0176 m/z; calcd mass, 549.0189. Mp: 151.2 °C. UPLC−MS (DAD/ESI): t_R = 6.21 min, for $C_{24}H_{23}Br_2FN_2O_2$ $[M + H]^+$ found, 549.16 m/z; calcd mass, 549.02.

*4-(3-Bromo-4-((2-bromo-3′-fluoro-[1,1′-biphenyl]-3-yl)methoxy)benzyl)thiomorpholine 1,1-Dioxide (**4l**).* The synthesis of compound **4l** was performed following the procedure of **2g**. Preparation included the use of **4i** (100 mg, 0.22 mmol), thiomorpholine 1,1-dioxide (133 mg, 0.99 mmol), $NaBH_3CN$ (64 mg, 1.08 mmol), AcOH (3 droplets), and anhydrous DMF (4.0 mL). The crude product was purified by column chromatography (silica gel, 0−10% MeOH in $CHCl_3$) to give an off-white solid (41 mg, yield: 33%) as a product. ^{1}H NMR (600 MHz, $CDCl_3$) δ: 7.75 (dd, J = 7.7, 0.7 Hz, 1H), 7.57 (d, J = 2.0 Hz, 1H), 7.41 (m, 2H), 7.28 (dd, J = 7.5, 1.5 Hz, 1H), 7.20 (dd, J = 8.4, 2.0 Hz, 1H), 7.16 (d, J = 7.6 Hz, 1H), 7.13−7.08 (m, 2H), 6.95 (d, J = 8.4 Hz, 1H), 5.25 (s, 2H), 3.58 (s, 2H), 3.08−3.05 (m, 4H), 2.99−2.96 (m, 4H). ^{13}C NMR (151 MHz, $CDCl_3$) δ: 162.4 (d, $^1J_{C-F}$ = 246.1 Hz), 154.4, 143.2 (d, $^3J_{C-F}$ = 7.9 Hz), 142.2, 136.8, 133.8, 131.7, 130.4, 129.7 (d, $^3J_{C-F}$ = 8.3 Hz), 129.0, 127.7, 127.7, 125.4, 121.6, 116.8 (d, $^2J_{C-F}$ = 22.0 Hz), 114.8 (d, $^2J_{C-F}$ = 21.0 Hz), 113.6, 112.7, 70.9, 60.5, 51.6, 50.7. IR (ATR): 3079, 2818, 1608, 1584, 1494, 1463, 1363, 1328, 1301, 1253, 1199, 1124, 1110 cm^{-1}. HRMS ESI−MS-q-TOF for $C_{24}H_{22}Br_2FNO_3S$ $[M + Na]^+$ found, 603.9573 m/z; calcd mass, 603.9569. Mp: 183.0 °C. UPLC−MS (DAD/ESI): t_R = 8.81 min, for $C_{24}H_{22}Br_2FNO_3S$ $[M + H]^+$ found, 582.13 m/z; calcd mass, 581.97.

https://dx.doi.org/10.1021/acs.jmedchem.0c01260
J. Med. Chem. 2020, 63, 11271−11285

*(3-((2-Bromo-3′-fluoro-[1,1′-biphenyl]-3-yl)methoxy)phenyl)-methanol (**4m**).* Compound **4m** was obtained following the protocol of **2a**, using **1f** (700 mg, 2.03 mmol), 3-(hydroxymethyl)phenol (252 mg, 2.03 mmol), potassium carbonate (562 mg, 4.07 mmol), and anhydrous DMF (10 mL). Crude product was purified by column chromatography on silica gel (0−100% AcOEt in hexane) and yielded **4m** (408 mg, 52%) as a white solid. ^{1}H NMR (600 MHz, $CDCl_3$) δ: 7.61−7.57 (m, 1H), 7.44−7.37 (m, 2H), 7.31 (t, J = 7.9 Hz, 1H), 7.27 (d, J = 1.7 Hz, 1H), 7.19−7.16 (m, 1H), 7.14−7.08 (m, 2H), 7.07 (s, 1H), 7.00 (dd, J = 7.5, 0.6 Hz, 1H), 6.95 (dd, J = 8.2, 2.4 Hz, 1H), 5.21 (s, 2H), 4.70 (d, J = 5.8 Hz, 2H), 1.73 (t, J = 6.0 Hz, 1H). ^{13}C NMR (151 MHz, $CDCl_3$) δ: 162.4 (d, $^1J_{C-F}$ = 246.2 Hz), 158.9, 143.4 (d, $^3J_{C-F}$ = 7.9 Hz), 142.8, 142.3, 137.4, 130.5, 129.9, 129.7 (d, $^3J_{C-F}$ = 8.3 Hz), 128.1, 127.5, 125.4 (d, $^4J_{C-F}$ = 2.3 Hz), 122.4, 119.9, 116.8 (d, $^2J_{C-F}$ = 22.0 Hz), 114.7 (d, $^2J_{C-F}$ = 21.0 Hz), 114.2, 113.5, 70.2, 65.4. IR (ATR): 3233, 2854, 1601, 1584, 1493, 1448, 1417, 1365, 1258, 1196, 1173, 1155, 1068, 1055 cm^{-1}. HRMS ESI−MS-q-TOF for $C_{20}H_{16}BrFO_2$ $[M + Na]^+$ found, 409.0207 m/z; calcd mass, 409.0215. Mp: 59.0 °C. UPLC−MS (DAD/ESI): t_R = 8.05 min, for $C_{20}H_{16}BrFO_2$ $[(M - H_2O) + H]^+$ found, 369.17 m/z; calcd mass, 369.02.

*4-(3-((2-Bromo-3′-fluoro-[1,1′-biphenyl]-3-yl)methoxy)benzyl)-thiomorpholine 1,1-Dioxide (**4n**).* Compound **4m** (100 mg, 0.26 mmoL) was dissolved in anhydrous DCM (3 mL) under Ar. $SOCl_2$ (1.0 mL) was added carefully, and the resulted mixture was stirred at 45 °C for 3 h. Afterward, the reaction was stopped, and the mixture was concentrated under reduced pressure. Generated in situ chloride, thiomorpholine 1,1-dioxide (105 mg, 0.78 mmol), and K_2CO_3 (178 mg, 1.29 mmol) were stirred in anhydrous DMF (5 mL) at room temperature overnight. The solvent was removed under reduced pressure. Water was added (30 mL), and the mixture was extracted with AcOEt (2 × 30 mL). Organic layers were combined and concentrated. The crude product was chromatographed on silica gel eluting with 0−60% AcOEt in hexane to give 38 mg of an off-white solid with a yield of 29%. ^{1}H NMR (600 MHz, $CDCl_3$) δ: 7.58 (dd, J = 7.6, 1.0 Hz, 1H), 7.44−7.37 (m, 2H), 7.31−7.27 (m, 2H), 7.17 (d, J = 7.6 Hz, 1H), 7.13−7.08 (m, 2H), 6.99 (s, 1H), 6.94 (m, 2H), 5.20 (s, 2H), 3.65 (s, 2H), 3.08−3.03 (m, 4H), 2.99 (m, 4H). ^{13}C NMR (151 MHz, $CDCl_3$) δ: 162.4 (d, $^1J_{C-F}$ = 246.2 Hz), 158.9, 143.3 (d, $^3J_{C-F}$ = 8.0 Hz), 142.4, 139.3, 137.3, 130.5, 129.9, 129.7 (d, $^3J_{C-F}$ = 8.3 Hz), 128.1, 127.5, 125.4, 122.4, 121.7, 116.8 (d, $^2J_{C-F}$ = 22.0 Hz), 115.5, 114.8 (d, $^2J_{C-F}$ = 20.9 Hz), 114.0, 70.2, 61.5, 51.7, 50.8. IR (ATR): 2918, 2849, 1583, 1487, 1462, 1364, 1290, 1269, 1195, 1153, 1123, 1049 cm^{-1}. HRMS ESI−MS-q-TOF for $C_{24}H_{23}BrFNO_3S$ $[M + Na]^+$ found, 526.0454 m/z; calcd mass, 526.0464. Mp: 94.2 °C. UPLC−MS (DAD/ESI): t_R = 8.28 min, for $C_{24}H_{23}BrFNO_3S$ $[M + H]^+$ found, 504.17 m/z; calcd mass, 504.06.

■ ASSOCIATED CONTENT

Supporting Information

The Supporting Information is available free of charge at https://pubs.acs.org/doi/10.1021/acs.jmedchem.0c01260.

Biochemical characterization of tested compounds; AIDA-NMR 2D HSQC (A−F) and 1D NMR spectra (G); ELISA assay results; the aliphatic part of the ^{1}H NMR spectrum of apo-PD-L1 (blue) and PD-L1 with compound **2k** (red) and compound **3d** (green) compounds in the molar ratio 1:1; cytotoxicity assay of tested compounds in the range of 0.02−100 μM final concentration; MST results; preparation of substrates and description of synthesis of short fragment **1a−g**; copies of NMR spectra; and LCMS analysis for key compounds (PDF)

Molecular formula strings and biological data for final compounds (CSV)

■ AUTHOR INFORMATION

Corresponding Authors

Tad A. Holak − *Faculty of Chemistry, Jagiellonian University, Krakow 30-387, Poland*; Email: tadholak@uj.edu.pl

Jacek Plewka − *Faculty of Chemistry, Jagiellonian University, Krakow 30-387, Poland*; orcid.org/0000-0002-0307-0907; Email: jacek.plewka@uj.edu.pl

Authors

Magdalena Konieczny − *Faculty of Chemistry, Jagiellonian University, Krakow 30-387, Poland*; orcid.org/0000-0002-0207-6821

Bogdan Musielak − *Faculty of Chemistry, Jagiellonian University, Krakow 30-387, Poland*; orcid.org/0000-0002-1665-5920

Justyna Kocik − *Faculty of Chemistry, Jagiellonian University, Krakow 30-387, Poland*; orcid.org/0000-0002-3779-3118

Lukasz Skalniak − *Faculty of Chemistry, Jagiellonian University, Krakow 30-387, Poland*; orcid.org/0000-0002-6707-6697

Dominik Sala − *Faculty of Chemistry, Jagiellonian University, Krakow 30-387, Poland*; orcid.org/0000-0002-9417-9149

Miroslawa Czub − *Faculty of Chemistry, Jagiellonian University, Krakow 30-387, Poland*

Katarzyna Magiera-Mularz − *Faculty of Chemistry, Jagiellonian University, Krakow 30-387, Poland*; orcid.org/0000-0002-4826-6380

Ismael Rodriguez − *Faculty of Chemistry, Jagiellonian University, Krakow 30-387, Poland*; orcid.org/0000-0001-9722-610X

Maja Myrcha − *Faculty of Chemistry, Jagiellonian University, Krakow 30-387, Poland*

Malgorzata Stec − *Department of Clinical Immunology, Institute of Pediatrics, Jagiellonian University Medical College, Krakow 30-663, Poland*; orcid.org/0000-0003-2063-9939

Maciej Siedlar − *Department of Clinical Immunology, Institute of Pediatrics, Jagiellonian University Medical College, Krakow 30-663, Poland*; orcid.org/0000-0002-3904-5412

Complete contact information is available at: https://pubs.acs.org/10.1021/acs.jmedchem.0c01260

Funding

This research was funded (to T.A.H.) by the project POIR.04.04.00-00-420F/17-00, which is carried out within the TEAM program of the Foundation for Polish Science cofinanced by the European Union under the European Regional Development Fund and partially by the Grant Symphony UMO-2014/12/W/NZ1/00457 from the National Science Centre, Poland.

Notes

The authors declare no competing financial interest.

■ ACKNOWLEDGMENTS

J.K. acknowledges the support of InterDokMed project no. POWR.03.02.00-00-I013/16.

■ ABBREVIATIONS USED

PD-1, programmed cell death protein; PD-L1, programmed cell death protein ligand; mAbs, monoclonal antibodies; irAEs immune, related adverse events; w-AIDA-NMR, weak-antagonist-induced dissociation assay NMR; SAR, structure−activity relationship; IC_{50}, half maximal inhibitory concentration; EC_{50}, half maximal effective concentration; HTRF, homogeneous time-resolved fluorescence; TCR, T cell receptor; DMSO, dimethyl sulfoxide

REFERENCES

(1) Pardoll, D. M. The Blockade of Immune Checkpoints in Cancer Immunotherapy. *Nat. Rev. Cancer* **2012**, *12* (4), 252−264.

(2) Dömling, A.; Holak, T. A. Programmed Death-1: Therapeutic Success after More than 100 Years of Cancer Immunotherapy. *Angew. Chem., Int. Ed.* **2014**, *53* (9), 2286−2288.

(3) Ledford, H.; Else, H.; Warren, M. Cancer Immunologists Scoop Medicine Nobel Prize. *Nature* **2018**, *562* (7725), 20−21.

(4) Hoos, A. Development of Immuno-Oncology Drugs — from CTLA4 to PD1 to the next Generations. *Nat. Rev. Drug Discovery* **2016**, *15* (4), 235−247.

(5) Mahoney, K. M.; Rennert, P. D.; Freeman, G. J. Combination Cancer Immunotherapy and New Immunomodulatory Targets. *Nat. Rev. Drug Discovery* **2015**, *14* (8), 561−584.

(6) Sharma, P.; Allison, J. P. The Future of Immune Checkpoint Therapy. *Science (Washington, DC, U. S.)* **2015**, *348* (6230), 56−61.

(7) Shin, D. S.; Ribas, A. The Evolution of Checkpoint Blockade as a Cancer Therapy: What's Here, What's Next? *Curr. Opin. Immunol.* **2015**, *33*, 23−35.

(8) Topalian, S. L.; Drake, C. G.; Pardoll, D. M. Immune Checkpoint Blockade: A Common Denominator Approach to Cancer Therapy. *Cancer Cell* **2015**, *27* (4), 450−461.

(9) Hellmann, M. D.; Paz-Ares, L.; Bernabe Caro, R.; Zurawski, B.; Kim, S.-W.; Carcereny Costa, E.; Park, K.; Alexandru, A.; Lupinacci, L.; de la Mora Jimenez, E.; Sakai, H.; Albert, I.; Vergnenegre, A.; Peters, S.; Syrigos, K.; Barlesi, F.; Reck, M.; Borghaei, H.; Brahmer, J. R.; O'Byrne, K. J.; Geese, W. J.; Bhagavatheeswaran, P.; Rabindran, S. K.; Kasinathan, R. S.; Nathan, F. E.; Ramalingam, S. S. Nivolumab plus Ipilimumab in Advanced Non−Small-Cell Lung Cancer. *N. Engl. J. Med.* **2019**, *381* (21), 2020−2031.

(10) Checkpoint Inhibitors: Global Markets; https://www.bccresearch.com/market-research/pharmaceuticals/checkpoint-inhibitors-global-markets.html (accessed Oct 23, 2019).

(11) Alsaab, H. O.; Sau, S.; Alzhrani, R.; Tatiparti, K.; Bhise, K.; Kashaw, S. K.; Iyer, A. K. PD-1 and PD-L1 Checkpoint Signaling Inhibition for Cancer Immunotherapy: Mechanism, Combinations, and Clinical Outcome. *Front. Pharmacol.* **2017**, *8*, 1 DOI: 10.3389/fphar.2017.00561.

(12) Acúrcio, R. C.; Scomparin, A.; Conniot, J.; Salvador, J. A. R.; Satchi-Fainaro, R.; Florindo, H. F.; Guedes, R. C. Structure-Function Analysis of Immune Checkpoint Receptors to Guide Emerging Anticancer Immunotherapy. *J. Med. Chem.* **2018**, *61* (24), 10957−10975.

(13) Tang, J.; Shalabi, A.; Hubbard-Lucey, V. M. Comprehensive Analysis of the Clinical Immuno-Oncology Landscape. *Ann. Oncol.* **2018**, *29* (1), 84−91.

(14) Farid, S. S. Process Economics of Industrial Monoclonal Antibody Manufacture. *J. Chromatogr. B: Anal. Technol. Biomed. Life Sci.* **2007**, *848* (1), 8−18.

(15) Baldo, B. Adverse Events to Monoclonal Antibodies Used for Cancer Therapy: Focus on Hypersensitivity Responses. *Oncoimmunology* **2013**, *2* (10), e26333.

(16) Adams, J. L.; Smothers, J.; Srinivasan, R.; Hoos, A. Big Opportunities for Small Molecules in Immuno-Oncology. *Nat. Rev. Drug Discovery* **2015**, *14* (9), 603−622.

(17) Shaabani, S.; Huizinga, H. P. S.; Butera, R.; Kouchi, A.; Guzik, K.; Magiera-Mularz, K.; Holak, T. A.; Dömling, A. A Patent Review on PD-1/PD-L1 Antagonists: Small Molecules, Peptides, and Macrocycles (2015−2018). *Expert Opin. Ther. Pat.* **2018**, *28* (9), 665−678.

(18) Guzik, K.; Tomala, M.; Muszak, D.; Konieczny, M.; Hec, A.; Błaszkiewicz, U.; Pustuła, M.; Butera, R.; Dömling, A.; Holak, T. A. Development of the Inhibitors That Target the PD-1/PD-L1 Interaction—A Brief Look at Progress on Small Molecules, Peptides and Macrocycles. *Molecules* **2019**, *24* (11), 2071.

(19) Qin, M.; Cao, Q.; Wu, X.; Liu, C.; Zheng, S.; Xie, H.; Tian, Y.; Xie, J.; Zhao, Y.; Hou, Y.; Zhang, X.; Xu, B.; Zhang, H.; Wang, X. Discovery of the Programmed Cell Death-1/Programmed Cell Death-Ligand 1 Interaction Inhibitors Bearing an Indoline Scaffold. *Eur. J. Med. Chem.* **2020**, *186*, 111856.

(20) Qin, M.; Cao, Q.; Zheng, S.; Tian, Y.; Zhang, H.; Xie, J.; Xie, H.; Liu, Y.; Zhao, Y.; Gong, P. Discovery of [1,2,4]Triazolo[4,3-a]Pyridines as Potent Inhibitors Targeting the Programmed Cell Death-1/Programmed Cell Death-Ligand 1 Interaction. *J. Med. Chem.* **2019**, *62*, 4703.

(21) Musielak, B.; Kocik, J.; Skalniak, L.; Magiera-Mularz, K.; Sala, D.; Czub, M.; Stec, M.; Siedlar, M.; Holak, T. A.; Plewka, J. CA-170 − A Potent Small-Molecule PD-L1 Inhibitor or Not? *Molecules* **2019**, *24* (15), 2804.

(22) Blevins, D. J.; Hanley, R.; Bolduc, T.; Powell, D. A.; Gignac, M.; Walker, K.; Carr, M. D.; Hof, F.; Wulff, J. E. *In Vitro* Assessment of Putative PD-1/PD-L1 Inhibitors: Suggestions of an Alternative Mode of Action. *ACS Med. Chem. Lett.* **2019**, *10*, 1187.

(23) Ganesan, A.; Ahmed, M.; Okoye, I.; Arutyunova, E.; Babu, D.; Turnbull, W. L.; Kundu, J. K.; Shields, J.; Agopsowicz, K. C.; Xu, L.; Tabana, Y.; Srivastava, N.; Zhang, G.; Moon, T. C.; Belovodskiy, A.; Hena, M.; Kandadai, A. S.; Hosseini, S. N.; Hitt, M.; Walker, J.; Smylie, M.; West, F. G.; Siraki, A. G.; Lemieux, M. J.; Elahi, S.; Nieman, J. A.; Tyrrell, D. L.; Houghton, M.; Barakat, K. Comprehensive in Vitro Characterization of PD-L1 Small Molecule Inhibitors. *Sci. Rep.* **2019**, *9* (1), 1 DOI: 10.1038/s41598-019-48826-6.

(24) Zak, K. M.; Grudnik, P.; Guzik, K.; Zieba, B. J.; Musielak, B.; Dömling, A.; Dubin, G.; Holak, T. A. Structural Basis for Small Molecule Targeting of the Programmed Death Ligand 1 (PD-L1). *Oncotarget* **2016**, *7* (21), 30323−30335.

(25) Musielak, B.; Janczyk, W.; Rodriguez, I.; Plewka, J.; Sala, D.; Magiera-Mularz, K.; Holak, T. Competition NMR for Detection of Hit/Lead Inhibitors of Protein−Protein Interactions. *Molecules* **2020**, *25* (13), 3017.

(26) Krajewski, M.; Rothweiler, U.; D'Silva, L.; Majumdar, S.; Klein, C.; Holak, T. A. An NMR-Based Antagonist Induced Dissociation Assay for Targeting the Ligand−Protein and Protein−Protein Interactions in Competition Binding Experiments. *J. Med. Chem.* **2007**, *50* (18), 4382−4387.

(27) Skalniak, L.; Zak, K. M.; Guzik, K.; Magiera, K.; Musielak, B.; Pachota, M.; Szelazek, B.; Kocik, J.; Grudnik, P.; Tomala, M.; Krzanik, S.; Pyrc, K.; Dömling, A.; Dubin, G.; Holak, T. A. Small-Molecule Inhibitors of PD-1/PD-L1 Immune Checkpoint Alleviate the PD-L1-Induced Exhaustion of T-Cells. *Oncotarget* **2017**, *8* (42), 72167−72181.

(28) Trott, O.; Olson, A. J. AutoDock Vina: Improving the Speed and Accuracy of Docking with a New Scoring Function, Efficient Optimization, and Multithreading. *J. Comput. Chem.* **2009**, *31*, 455−461.

(29) Dallakyan, S.; Olson, A. J. Small-Molecule Library Screening by Docking with PyRx. *Methods in Molecular Biology*; Humana Press: New York, 2015; Vol. *1263*, pp 243−250.

(30) Cunningham, R. A.; Holland, M.; McWilliams, E.; Hodi, F. S.; Severgnini, M. Detection of Clinically Relevant Immune Checkpoint Markers by Multicolor Flow Cytometry. *J. Biol. Methods* **2019**, *6* (2), 114.

(31) Salentin, S.; Schreiber, S.; Haupt, V. J.; Adasme, M. F.; Schroeder, M. PLIP: Fully Automated Protein−Ligand Interaction Profiler. *Nucleic Acids Res.* **2015**, *43* (W1), W443−W447.

(32) Zak, K. M.; Kitel, R.; Przetocka, S.; Golik, P.; Guzik, K.; Musielak, B.; Dömling, A.; Dubin, G.; Holak, T. A. Structure of the Complex of Human Programmed Death 1, PD-1, and Its Ligand PD-L1. *Structure* **2015**, *23* (12), 2341−2348.

(33) Van Kuppeveld, F. J. M.; Van der Logt, J. T. M.; Angulo, A. F.; Van Zoest, M. J.; Quint, W. G. V; Niesters, H. G. M.; Galama, J. M. D.; Melchers, W. J. G. Genus- and Species-Specific Identification of Mycoplasmas by 16S RRNA Amplification. *Appl. Environ. Microbiol.* **1992**, *58* (8), 2606−2615.

https://dx.doi.org/10.1021/acs.jmedchem.0c01260
J. Med. Chem. 2020, 63, 11271−11285